

Title: Dopamine differentially affects retinal circuits to shape the retinal code

Running title: Dopamine's distinct effects on retinal circuits

Authors: Rebekah A. Warwick^{1*}, Alina S. Heukamp^{1*}, Serena Riccitelli¹ and Michal Rivlin-Etzion¹

¹Department of Brain Sciences, Weizmann Institute of Science, 234 Herzl Street, Rehovot
7610001, Israel

* These authors contributed equally.

Correspondence: Michal Rivlin-Etzion (michal.rivlin@weizmann.ac.il, ORCID: 0000-0002-1310-3370)

Keywords: Retina, Retinal ganglion cells, Dopamine, Apomorphine, Centre-surround receptive field, Multielectrode array, transient Off- α RGC

First Author Profile

Rebekah Warwick obtained her PhD at the Hebrew University of Jerusalem and conducted her postdoctoral research in Michal Rivlin's lab at the Weizmann Institute. She is interested in retinal computations and how they are affected by neuromodulators.

Alina Heukamp obtained her M.Sc. at the IMPRS for Neurosciences in Göttingen, Germany. She is currently a PhD student in the lab of Michal Rivlin and is interested in computations in the retina and beyond.

Key points summary

- Receptive fields of retinal ganglion cells (RGCs) have a center-surround organisation and previous work has shown that this organisation can be modulated by dopamine in a light-intensity dependent manner.
- Dopamine is thought to enhance RGCs' antagonistic surround, but a detailed understanding of how different RGC subtypes are affected is missing.
- Using a multielectrode array recordings, clustering analysis and pharmacological manipulations, we found that dopamine can either enhance or weaken antagonistic surrounds, and also change response kinetics, of RGCs in a subtype-specific manner.

This is an Accepted Article that has been peer-reviewed and approved for publication in the The Journal of Physiology, but has yet to undergo copy-editing and proof correction. Please cite this article as an 'Accepted Article'; [doi: 10.1113/JP284215](https://doi.org/10.1113/JP284215).

This article is protected by copyright. All rights reserved.

- We performed targeted patch-clamp recordings of one RGC subtype, the transient-Off- α RGC, and identified the underlying circuits via which dopamine shapes its receptive field.
- Our findings demonstrate that dopamine acts in a subtype-specific manner and can have complex effects, which has implications for other retinal computations that rely on receptive field structure.

Abstract

Dopamine has long been reported to enhance antagonistic surrounds of retinal ganglion cells (RGCs). Yet, the retina contains many different RGC subtypes and the effects of dopamine can be subtype-specific. Using multielectrode array (MEA) recordings we investigated how dopamine shapes the receptive fields of RGCs in the mouse retina. We found that the non-selective dopamine receptor agonist, apomorphine, can either increase or decrease RGCs' surround strength, depending on their subtype. We used two-photon targeted patch-clamp to target a specific RGC subtype, the transient-Off- α RGC. In line with our MEA recordings, apomorphine did not increase the antagonistic surround of transient-Off- α RGCs but enhanced their responses to Off stimuli in the centre receptive field. Both D_1 - and D_2 -like family receptor (D_1 -R and D_2 -R) blockers had the opposite effect and reduced centre-mediated responses, but differently affected transient-Off- α RGC's surround. While D_2 -R blocker reduced surround antagonism, D_1 -R blocker led to surround activation, revealing On responses to large stimuli. Using voltage-clamp recordings we separated excitatory inputs from Off cone bipolar cells and inhibitory inputs from the primary rod pathway. In control conditions, cone inputs displayed strong surround antagonism, while inputs from the primary rod pathway showed no surround. Yet, the surround activation in the D_1 -R blockade originated from the primary rod pathway. Our findings demonstrate that dopamine differentially affects RGC subtypes via distinct

This article is protected by copyright. All rights reserved.

pathways, suggesting that dopamine has a more complex role in shaping the retinal code than previously reported.

Introduction

The retina employs multiple strategies to operate over a large range of light levels (Fein & Szuts 1982, Rivlin-Etzion et al. 2018, Shapley & Enroth-Cugell 1984). Specialised rod and cone photoreceptors support vision across large ranges of light intensity, and horizontal cells, bipolar cells and amacrine cells exhibit functional changes as light intensity increases (Dunn et al. 2006, 2007; Flood & Eggers 2021, Flood et al. 2018, Mazade & Eggers 2013, 2016, 2020; Shapley & Enroth-Cugell 1984, Xin & Bloomfield 1999). Consequently, the output of retinal ganglion cells (RGCs) is also light intensity-dependent (Barlow et al. 1957, Dedek et al. 2008, Farrow et al. 2013, Pearson & Kerschensteiner 2015, Tikidji-Hamburyan et al. 2015). A single signalling molecule, dopamine, has been credited with inducing many of these light-dependent changes (Flood et al. 2018, Godley & Wurtman 1988, Goel & Mangel 2021, Herrmann et al. 2011, Hu et al. 2010, Kothmann et al. 2009, Mazade et al. 2019). Dopamine is released from the dopaminergic amacrine cell and its levels increase with light intensity (Bauer et al. 1980, Godley & Wurtman 1988, Pérez-Fernández et al. 2019, Witkovsky 2004). Rod photoreceptors were shown to contribute to this process, suppressing release at low intensities and enhancing it at high light intensities (Pérez-Fernández et al. 2019).

All dopamine receptor subtypes are G-protein coupled receptors, however, activation of D₁-like family receptors (D₁-R) leads to an increase in cAMP, whereas activation of D₂-like family

This article is protected by copyright. All rights reserved.

receptors (D_2 -R) leads to a decrease in cAMP (Witkovsky 2004). D_1 -R are expressed on horizontal, bipolar and amacrine cells (Farshi et al. 2016, Herrmann et al. 2011, Kothmann et al. 2009, Mazade & Eggers 2020, Nguyen-Legros et al. 1999, Veruki & Wässle 1996), and D_2 -R are expressed on rod and cone photoreceptors as well as the dopaminergic amacrine cell (Muresan & Besharse 1993, Veruki 1997). RGCs have been reported to express both types ((Koulen 1999, Ogata et al. 2012, Tran et al. 2019), Single Cell Portal (SCP), Broad Institute). In all retinal cell types, the expression is selective to both cell- and receptor-subtype. With dopamine receptors expressed throughout the retina, but dopaminergic amacrine cell processes mostly confined to the border of the inner plexiform and inner nuclear layers, the majority of dopamine signalling occurs in a paracrine fashion (Witkovsky 2004).

A primary effect of dopamine on RGCs is to modulate their receptive field organisation. RGCs typically exhibit antagonistic centre-surround receptive fields, where the polarity of the surround is opposite to that of the centre. For example, a light stimulus presented solely in the centre of an On RGC's receptive field will elicit an On response. However, a light stimulus that includes its surround may have two effects: first, it may elicit an On response of reduced amplitude (a phenomenon termed 'surround antagonism', see Fig. 1A, top). Second, it may cause a response of opposite polarity to that of the centre, in this case an Off response (a phenomenon termed 'surround activation', see Fig. 1A, middle) (Chaffiol et al. 2017). RGCs with no surround will display similar responses to centre and full-field stimulation (Fig. 1A, bottom). Early studies investigating the effects of dopamine on RGCs' receptive fields found that blocking dopamine in light-adapted retinas weakened surround receptive fields (Jensen 1991; Jensen & Daw 1984, 1986). These studies were carried out on randomly selected RGCs that were clustered into groups based on their centre responses (On, Off and On-Off) and response kinetics (sustained or transient). Today we know that

This article is protected by copyright. All rights reserved.

there are many more RGC subtypes, for example, the mouse retina contains more than 30 different ones (Baden et al. 2016, Masland 2012). Since each RGC subtype collects inputs from distinct sets of interneurons, different circuits may underlie their surround receptive fields (Farrow et al. 2013), and they may be differentially affected by dopamine.

Here, we used multielectrode array (MEA) recordings of RGCs to gain an understanding of how the dopamine receptor agonist apomorphine differentially shapes receptive fields of different subtypes of RGCs. After clustering RGCs into functional subtypes, we identified several subtypes that exhibit either a weakened or strengthened surround with a dopamine receptor agonist. Guided by the results from our clustering, we then utilised the advancement of genetically labelled RGC subtypes to target one subtype, the transient-Off- α RGC (tOff- α RGC; Huberman et al. (2008)). tOff- α RGCs receive input from Off cone bipolar cells and the primary rod pathway (Manookin et al. 2008). Using extracellular and intracellular recordings we found that apomorphine enhanced the centre response in tOff- α RGCs while having a differential effect on their surround, increasing surround antagonism of cone inputs but not of inputs from the primary rod pathway. Together, our findings suggest that dopamine's role in shaping RGC receptive fields is more complex than simply surround strengthening. Instead, dopamine's effects on centre-surround receptive fields are pathway-specific.

Methods

Ethical Approval

All experimental procedures were approved by the Institutional Animal Care and Use Committee (IACUC) at the Weizmann Institute of Science (00860120-2).

This article is protected by copyright. All rights reserved.

Animals

Calb2-EGFP mice, in which tOff-αRGCs express GFP, were obtained from Mutant Mouse Regional Resource Center (https://www.mmrrc.org/catalog/sds.php?mmrrc_id=283) (Gong et al. 2003, Huberman et al. 2008) and crossed to C57BL/6J0laHsd. The percentage of labelled tOff-αRGCs varied between the mice, and while some showed a mosaic of tOff-αRGCs, others labelled only a portion of them. For MEA recordings, wildtype mice from the same colony were used. Mice were kept on a 12:12 h light-dark cycle with free access to food and water. Mice of either sex were used.

Tissue preparation

Mice (4-20 weeks old) were deeply anaesthetised with isoflurane and decapitated. Retinas were isolated under dim red and infra-red (IR) illumination in oxygenated Ames' medium (Sigma, St. Louis, MO, USA). The orientation of the retinas was based on landmarks in the choroid, as previously described (Wei et al. 2010).

For patch clamp recordings, dorsal retinas were isolated from the pigment epithelium and mounted photoreceptor side down over a hole of 1–1.5 mm² on filter paper, centred over the retina piece (GSWP01300, Merck Millipore, Billerica, MA, USA). Retinas were kept in the dark at room temperature in Ames' medium bubbled with 95% O₂/5% CO₂ until use (maximum 5 h).

For MEA experiments, the retina was mounted on an MEA as previously described (Warwick et al. 2022). In short, the MEA was coated with poly-D-lysine solution (PDL, 1.0 mg/ml in H₂O, Merck-

Millipore, CAT: A-003-E) for 1 hour. After washing off the PDL, the dorsal half of the retina was mounted with the RGC layer facing the electrodes as previously described in Karamanlis et al. (2021).

Multielectrode array (MEA) recordings

MEAs were purchased from MultiChannel Systems (252 electrodes, 8 μm electrode diameter, 30 μm minimal electrode distance, covering an area of $450\times 450\mu\text{m}$). The MEA was placed in the headstage with constant perfusion of oxygenated Ames' medium (flow rate: 3.5 ml/min) and a heating pad below maintained a temperature of 33.2°C . Data acquisition was started one hour after placing the retina in the chamber to let the retina adapt. Extracellular voltage signals were amplified and digitised at 20 kHz and saved for offline analysis. In experiments where apomorphine (10 μM ; Cat# 2073, Tocris, UK) was used, a TTL pulse was recorded to determine the time point of changing the solution. Apomorphine was washed in for 15 mins before we presented visual stimuli again, and washed out for 30 mins. Control experiments were performed in a similar way to study changes over time, but without adding any drug.

Light stimuli for MEA experiments

Visual stimuli were generated in a custom-written GUI in Matlab (Psychophysics Toolbox, (Brainard 1997, Pelli 1997) and were projected via a monochromatic OLED display (eMagin, EMA-100309-01 SVGA+, 600 \times 800 pixels, 60 Hz refresh rate) and focussed on the photoreceptor layer via a telecentric lens (Edmund Optics, 2.0X, #58-431), resulting in a pixel size of 7.5 μm on the retina. At maximum brightness, the irradiance was $2.6 \mu\text{W}/\text{cm}^2$, resulting in 2.43×10^4 mouse rod isomerizations ($R^*\text{rod}^{-1}\text{s}^{-1}$, corresponding to the photopic regime), whereas the minimum brightness was $7.04\times 10^1 R^*\text{rod}^{-1}\text{s}^{-1}$.

This article is protected by copyright. All rights reserved.

We presented several stimuli to probe the cells' centre-surround receptive field structure. For determining receptive fields, we presented a checkerboard white noise stimulus consisting of black and white squares of 60 μm size, changing at 30 Hz at equal probability, for 15 minutes. We used full-field spots (1200 μm diameter) and squares of different sizes (75 μm , 150 μm). We used full-field stimuli of three different contrasts: a white spot on black background, a white spot on grey background, and a black spot on grey background. Each of these consisted of 3 s baseline, 2 s presentation of the spot, followed by 3 s of baseline. The square stimulus consisted of white squares on a black background that were presented for 1 s in each position in a random order, one after the other. Squares of 75 μm size were presented in 196 different positions (on a 14 \times 14 grid), and squares of 150 μm size were presented in 64 positions (on an 8 \times 8 grid). For clustering the RGCs, we used a full-field stimulus consisting of contrast steps with each intensity presented for 2 s, followed by a contrast and frequency chirp (adapted from (Baden et al. 2016), see Fig. 1C, top). To identify direction-selective cells, we presented moving square-wave gratings of 100% contrast with a spatial frequency of 397.5 μm , moving in 8 equidistant directions in a pseudo-random order at a speed of 795 $\mu\text{m}/\text{s}$ (2 Hz). All stimuli were preceded by 30 s background intensity to let the retina adapt. All stimuli (except for white noise) were presented for 5 repetitions.

Patch-clamp recordings

Retinas were placed under a two-photon microscope (Bruker, Billerica, MA, USA) equipped with a Mai-Tai laser (Spectra-physics, Santa Clara, CA, USA) and superfused with oxygenated Ames medium at 32-34°C. Identification of and recording from GFP+ cells was carried out as previously described (Rivlin-Etzion et al. 2011, Warwick et al. 2018). In short, GFP+ cells were identified using the two-

This article is protected by copyright. All rights reserved.

photon microscope laser at 920 nm to avoid bleaching of the photoreceptors. The inner limiting membrane above the targeted cell was dissected under the microscope with a glass electrode using IR illumination.

Loose-patch recordings (holding voltage set to “OFF”) were performed with a new glass electrode (3–5 M Ω) filled with Ames’ medium. Intracellular voltage-clamp recordings were carried out using glass electrodes (6–8 M Ω) filled with intracellular solution containing (in mM): CsMeSO₃ 110, NaCl 2.8, HEPES 20, EGTA 4, TEA-Cl 5, ATP-Mg 4, GTP-Na₃ 0.3, C₄H₈N₃Na₂O₅P 10 and C₁₆H₂₇N₂OBr 5; pH7.35. A giga-Ohm seal was obtained before breaking in. Data were acquired at 10 kHz and for whole-cell mode filtered at 2 kHz with a Multiclamp 700B amplifier (Molecular Devices, CA, USA) using pCLAMP 10 recording software and a Digidata 1550 digitizer (Molecular Devices).

For experiments in which the drugs apomorphine (10 μ M; Cat# 2073, Tocris, UK), raclopride (2.5 μ M; Cat# 1810, Tocris), SCH-23390 (1 μ M; Cat# 0925, Tocris) or L-AP4 (5 μ M; Cat# 0103, Tocris, UK) were used, the relevant drug was added to the Ames solution and perfused for 30 mins prior to recording from tOff- α RGCs. Stock concentrations of drugs were prepared on the same day and stored at 4°C until use.

A portion of the data collected for the control condition in the loose patch and voltage-clamp experiments was previously published (Warwick et al. 2018).

Light stimuli for patch clamp experiments

Stimuli were generated using MATLAB and the Psychophysics Toolbox (Brainard 1997, Pelli 1997). A white, monochromatic organic light-emitting display (OLED-XL, 800×600 pixel resolution, 85 Hz refresh rate, eMagin, Bellevue, WA, USA) was used for the visual stimuli. The spectrum of the OLED was previously published (Warwick et al. 2018). The display image was projected through a 20x water-immersion objective (UMPLFLN20xW; Olympus, Tokyo, Japan), via the side port of the microscope, centred on the soma of the recorded cell, and focused on the photoreceptor layer. The diameter of the entire display on the retina was 1 mm across. The visual stimulation consisted of a grey background for 2 s, followed by the appearance of a dark spot on the grey background, which lasted 2 s before the spot disappeared, leaving the same grey background for a further 2 s. Sizes of displayed spots ranged from 50 to 800 μm . Weber's contrast for the dark spot on the grey background was -0.85 . The light intensity of the grey screen was $6.4 \times 10^4 \text{ R}^* \text{rod}^{-1} \text{ s}^{-1}$. All retinas were kept in the dark until recording. After recording from one tOff- α RGC, the location of the next tOff- α RGC was chosen so that it had not been exposed to the light stimulus of the previous cell. A maximum of 3 cells were recorded from each retina.

Data analysis of MEA recordings

Spike sorting of MEA data was performed using Kilosort2.0 (Pachitariu et al. 2016, 2018) with manual curation in Phy (Rossant & Harris 2013, Rossant et al. 2016). We only included well-separated units in our analysis, as determined by consistent spike shapes, spike amplitude, and inter-spike interval histogram that revealed a refractory period.

To determine RGCs' receptive field size and location, we calculated the spike-triggered average (STA) from the white noise data as the average stimulus preceding a spike, extracted from a

time window of 500 ms before the spike in time steps of 20 ms. From the spike-triggered average, we extracted the stimulus frame with the highest peak-to-peak amplitude and fitted a 2D-Gaussian to the spatial component of the receptive field. The receptive field diameter was defined as 2 SD. The temporal component (shown in Fig. 1C) was extracted as the mean over all stimulus pixels included in the cell's receptive field centre. To find the position of the square (75 or 150 μm in size) that was closest to the cells' receptive field, we calculated the Euclidean distances between the centres of each presented square and the cells' receptive fields, and defined the 'centre square' as the square closest to the cell's receptive field centre (see Fig. 1B, bottom). From here on, we only considered the response to the square closest to each cell's receptive field centre.

Clustering of RGCs (described in the following section) was carried out on all non-direction selective RGCs. We calculated the normalised vector sum as $NVS = \frac{|\sum R_{\theta} e^{i\theta}|}{\sum R_{\theta}}$, where R_{θ} represents the mean spike count in direction ϑ , and a direction-selectivity index (DSI) as $DSI = \frac{R_{PD} - R_{ND}}{R_{PD} + R_{ND}}$, where R_{PD} represents the mean spike count in the preferred direction, defined as the direction closest to the angle of the normalised vector sum, and R_{ND} the response in the opposite direction. An orientation-selective index (OSI) was calculated as $OSI = \frac{R_{PO} - R_{NO}}{R_{PO} + R_{NO}}$, where R_{PO} and R_{NO} are the spike counts in the preferred and null orientation, respectively. Direction-selective cells were defined as cells with a $DSI \geq 0.3$, $NVS \geq 0.15$, $OSI < 0.3$ and mean firing rate ≥ 1 Hz in response to the grating stimulus, and were excluded in all further analyses.

To cluster RGCs into functional subtypes, we created a matrix of spike times consisting of the responses to different stimuli recorded in control conditions (no drug added). Out of the five

repetitions, we only used responses from the third repetition. We concatenated the responses to the 150 μm square located closest to each cell's receptive field centre (On and Off response at onset and offset of the square respectively, 2 s combined), the response to the full-field contrast steps (consisting of 5 intensities of 2 s each) and the contrast and frequency-modulated full-field chirp. For each cell, we calculated a response quality index (RQI) from the peri-stimulus time histogram (PSTH; using a bin width of 50 ms) as $RQI = \frac{\text{Var}[\langle R \rangle_r]_t}{\langle \text{Var}[R]_t \rangle_r}$ (Baden et al. 2016), where R is the response matrix of stimulus repetitions \times time bins, $\text{Var}[\]$ represents the variance and $\langle \ \rangle$ represents the mean over dimension t (time) or r (repetitions) as indicated. We only included responsive cells in our clustering algorithm, which we defined as cells with an RQI ≥ 0.35 and a Pearson correlation of the third repetition to its mean PSTH of > 0.55 . In total, we used 567 cells from 9 retinas.

We used the SPIKY algorithm (Kreuz et al. 2013, 2015) to obtain a pairwise dissimilarity matrix between spike trains of all cells. We then performed agglomerative hierarchical clustering using the Ward distance to create a dendrogram. After analysing the merging cost between successive steps and visual inspection, as well as after excluding clusters with < 20 cells, or clusters that contained cells from only a single retina, we obtained 15 functional clusters with distinct responses (Fig. 1C).

A second dataset of cells that were not presented with the chirp stimulus ($n=847$ cells from 11 retinas) were then sorted into the existing clusters based on the Pearson correlation of their response to different full-field stimuli with the mean responses of each cluster. For that, we calculated the peri-stimulus time histograms (PSTHs, bin width of 5 ms) in response to a full-field spot of three different contrasts (a stimulus that was not used for the clustering, but was common to

all cells). We then calculated the mean response of each cluster to the same stimuli and assigned each cell to the cluster with whose PSTH it had the highest correlation. Together, our final dataset included 1414 cells from 20 retinas.

After obtaining clusters, we could split each cluster into RGCs from apomorphine experiments and control experiments (no drug added) to study the effects of apomorphine on each cluster.

To calculate maximum firing rates, we calculated the PSTH in response to the full-field spot stimuli (three different contrasts, see above) and separated them into the On (light onset) and Off (light offset) response. For plots shown in Fig. 1D and Fig. 2, we used the firing rate in response to the full-field stimulus onset or offset according to the cluster's preferred polarity preference (On or Off, respectively). We present responses to a white spot on black background for On responses (e.g., Fig. 2A-C), and responses to a black spot on grey background for Off responses (e.g., Fig. 2G-I). PSTHs and raster plots (Fig. 1A, Fig. 2) are cropped to show 1 s of baseline before and after the spot. For the square stimulus, we considered the Off response as the response that occurred in 1 s after disappearance of the white square. For the example cells and clusters shown in Fig. 2, maximum firing rates are shown either during the On response (cluster #1; On cell), the Off response (cluster #15; Off cell), or both (cluster #4; On-Off cell). An On-Off index (OOI) was calculated as $OOI = (R_{ON} - R_{OFF}) / (R_{ON} + R_{OFF})$, where R_{ON} and R_{OFF} are the maximum firing rates during the On and Off response, respectively. This index was calculated for both square sizes and the full-field stimuli. For example, the example cell shown in Fig. 1A (middle) has an OOI > 0.3 in response to the centre 150 μm square stimulus, making it an On cell.

This article is protected by copyright. All rights reserved.

Spatial-selectivity indices (SSIs) were calculated as $SSI = (R_C - R_S) / (R_C + R_S)$, where R_C and R_S are the maximum firing rates during the centre and surround stimuli, respectively (Hoggarth et al. 2015). We calculated those values using maximal firing rates in response to the square stimuli (75 and 150 μm) as R_C , and the response to the full-field spot as R_S . We used the On or Off response according to each cluster's preferred polarity (determined by the OOI calculated in response to a full-field spot (white spot on black background); On response for $OOI \geq 0$, Off response for $OOI < 0$, Fig. 1E).

To quantify the response kinetics, we calculated the ratio between the firing rate that occurred 200 ms after the maximum and the peak firing rate, resulting in values between 0 and 1, where high values correspond to prolonged, sustained responses and low values to short, transient responses. This was done for On and Off responses according to each cell's preferred polarity as explained above.

Data analysis of patch clamp recordings

Electrophysiological data were analysed offline. For loose-patch clamp recordings, spike times were extracted after filtration using a 4 pole Butterworth bandpass filter between 80 and 2000 Hz. PSTHs of spiking activity were calculated from 5 repetitions using a bin width of 50 ms. The background activity was determined based on the 2 s period of the initial grey screen in each trial and used to calculate the mean baseline activity and its SD. Cells were defined as responsive if their firing rate exceeded the mean baseline + 3 SD. The bin with the highest frequency during the dark spot stimulus was used to calculate the maximum response. For intracellular recordings, traces were

averaged across 4 repeats. To quantify the response kinetics, we calculated the percentage of the peak response after 200 ms analogous to the MEA data.

The spatial selectivity index (SSI) was calculated as $(R_C - R_S) / (R_C + R_S)$ where R_C is the maximum firing rate of the centre response (defined as 50-400 μm) and R_S is the response to the largest stimulus (800 μm) (Hoggarth et al. 2015). Note that contrary to the MEA recordings, stimuli here are (a) centred on the cell's receptive field and (b) of a contrast that is preferred by tOff- α RGCs, so that values might differ between the two experimental setups, even for the same cell type.

Statistical analysis

For the MEA data, maximum firing rates and SSI values were compared using a two-tailed Wilcoxon signed rank test ($\alpha=0.05$). For patch clamp data, a two-sample t-test was used to compare the mean SSI of the different groups.

Two-sample t-test was used to compare the mean duration of Off responses for different groups. The Wilcoxon rank-sum test was used to compare groups of cells for each spot size. For comparisons in Fig. 5H, a Wilcoxon signed rank test was used. Statistical significance was accepted at $p < 0.05$.

Notation of p-values is according to * $p < 0.05$, ** $p < 0.01$, *** $p < 0.001$, **** < 0.0001 .

Numerical values are presented at mean \pm standard deviation (SD).

This article is protected by copyright. All rights reserved.

Results

Dopamine differentially affects RGC subtypes

To study whether dopamine differentially modulates the light responses of different RGC subtypes, we performed MEA recordings from adult dark-adapted mouse retinas. We used a white noise stimulus to determine the cells' receptive field (Chichilnisky 2001), and both full-field spots (1200 μm diameter) and smaller square stimuli (75 and 150 μm square size presented at multiple locations, Fig. 1B) to estimate the surround strength. In order to study effects of dopamine in a more systematic manner, we clustered RGCs into functional subtypes using the SPIKY algorithm to calculate a pairwise dissimilarity matrix between spike trains of RGCs and a subsequent hierarchical clustering method (Jouty et al. 2018; Kreuz et al. 2013, 2015). For the clustering, we used responses to small squares (150 μm) and full-field (1200 μm) spots, as well as varying contrasts and frequency-modulated stimuli (full-field 'chirp' (Baden et al. 2016); see Methods). We obtained 15 functional clusters that were uniquely characterised by their light responses (Fig. 1C). RGCs that were recorded only in response to full-field spots of different contrasts were added to the existing clusters based on PSTH similarity (see Methods). The polarity preference of each cluster was defined based on the On-Off index (OOI) in response to a full field spot (see Methods), and in the analysis below we focussed on each cluster's preferred polarity response (On response for On cells, Off response for Off cells).

This article is protected by copyright. All rights reserved.

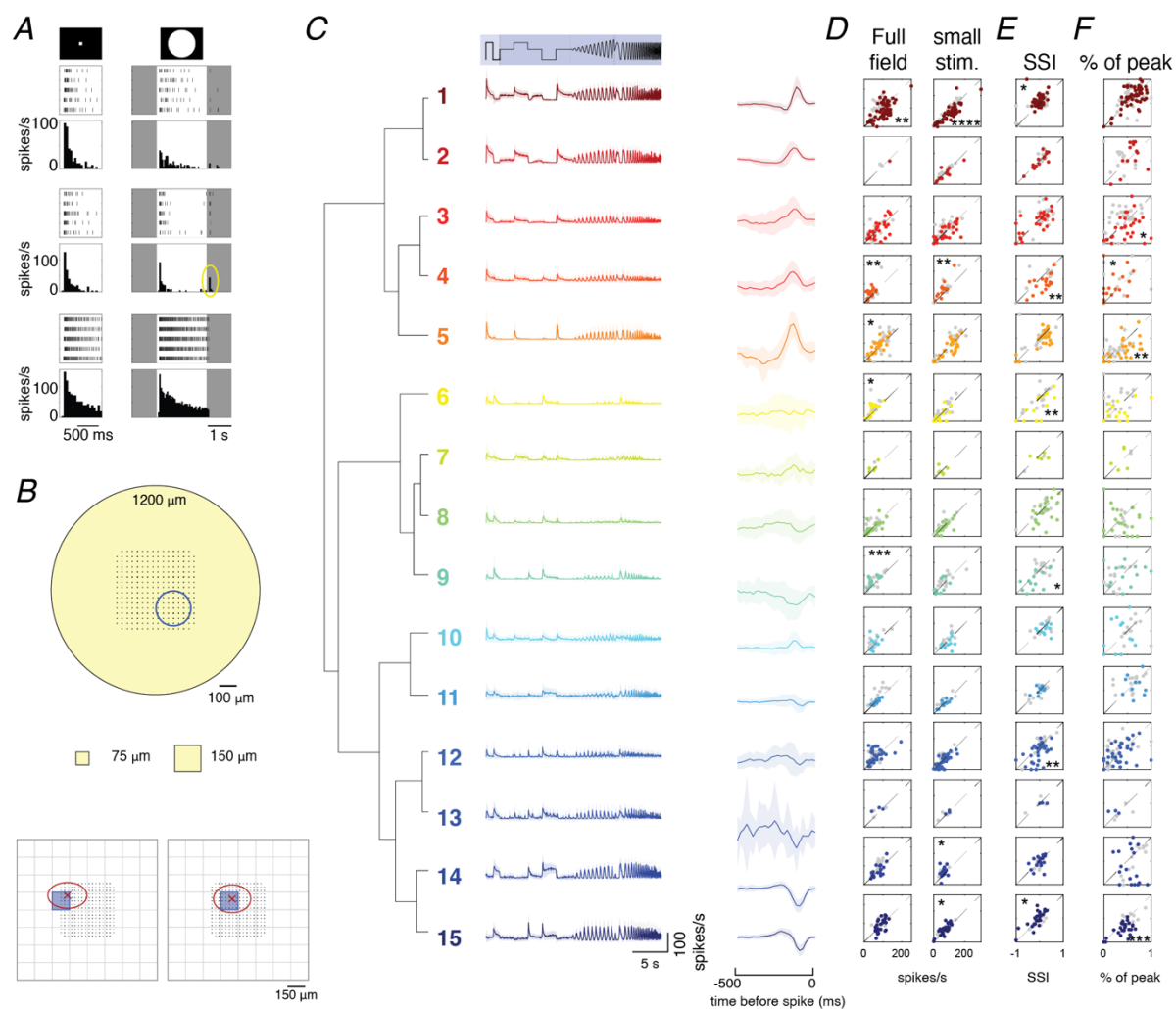


Figure 1. Clustering of RGCs into functional subtypes reveals complex effects of a dopamine receptor agonist on receptive field organisation. **A** Example of three different On-RGCs in response to a small (150 μm , left) and full-field (1200 μm , right) stimulus (shown in the first row). For each example, raster plot of 5 repetitions and PSTH are displayed. Top: a cell with a classical 'antagonistic surround'. Middle: a cell with 'surround activation' (note: this cell is an On cell (OOI for 150 μm square > 0.3) that displays an Off response (yellow circle) to a full-field stimulus). Bottom: a cell with no surround. **B** Top: Schematic of stimulus sizes used in MEA recordings. MEA is indicated by the black dots representing the electrodes. Blue circle shows an example receptive field with a diameter of 200 μm . Bottom: Receptive field outlines (red) of two example cells on the MEA, showing the location of the 150 μm square (blue) closest to the cell's receptive field centre (red cross). Grey grid shows positions of all presented squares. **C** Left: functional clusters of RGC subtypes with their PSTH (mean \pm SD). The stimulus is indicated above (light shaded: 150 μm , dark shaded: full-field). Right: temporal STA (mean \pm SD) to the white noise stimulus. Time below indicates time before spike. **D-F**

This article is protected by copyright. All rights reserved.

Comparison of maximum firing rate to full-field spots (1200 μm , left) and the closest square stimulus (75 or 150 μm , right) to each cell's receptive field centre (D), spatial-selectivity index (SSI; (E)), and response decay for full-field stimuli (F) in pre condition (x-axis) vs. apomorphine (y-axis). For each cluster, the maximum firing rate was extracted from the On or Off response according to the cluster's preferred polarity (see Methods). Data points indicate individual RGCs. Control cells from the same cluster (without adding apomorphine) are shown in grey. Scales of y axes are the same as x axes (labelled below) for D - F . * $p < 0.05$; ** $p < 0.01$, *** $p < 0.001$, **** $p < 0.0001$ according to Wilcoxon signed rank test. Asterisks above and below the unity line indicate increases and decreases with apomorphine, respectively.

Next, we aimed to investigate how dopamine alters the receptive field organisation of different RGC subtypes. Dopamine has long been reported to strengthen RGCs' surround (Herlinger et al. 1995, Jensen 1991, Jensen & Daw 1984, 1986; Witkovsky 2004). As dopamine is unstable in aqueous solutions (Herlinger et al. 1995), we chose to use apomorphine, a non-selective dopamine receptor agonist. At a concentration of 10 μM , apomorphine efficiently binds both D_1 - and D_2 -like family receptors despite having a higher affinity for the latter (Goldman & Keabian 1984). We investigated how application of apomorphine alters receptive fields of different clusters of RGCs. For that, we compared the maximum firing rates during small (75 μm , 150 μm) and full-field (1200 μm) stimuli in a control condition and after bath application of apomorphine. According to the classical view, dopamine-mediated increased surround antagonism would result in reduced firing rates in response to full-field spots (see example cell in Fig. 1A). Indeed, we found one cluster in which apomorphine significantly reduced maximum firing rates in response to full-field spots (Fig. 1D, cluster #1). We also found clusters with increased responses to full-field spots, suggesting a weakened surround (Fig. 1D, clusters #4, #5, #6 and #9). To quantify the relationship between centre and surround (full-field) responses, we calculated a spatial selectivity index (SSI, (Hoggarth et al. 2015)) as the normalised difference between each cell's centre and full-field responses, using either the On or Off response

This article is protected by copyright. All rights reserved.

according to each cluster's preferred polarity (see Methods). SSI values range from -1 to 1. A value of 1 indicates strong surround antagonism, with complete suppression of the response to a full-field stimulus; a value of 0 indicates the absence of any antagonistic surround; and a negative value indicates a stronger response to the full-field stimulus compared to a centre stimulus. As expected from responses to centre and full-field stimuli, the SSIs of multiple clusters of RGCs were altered by apomorphine, revealing either enhancement or reduction in surround strength (Fig. 1E, clusters #1, #4, #6, #9, #12 and #15). In addition, we noticed that a few of the clusters changed the kinetics of their responses with apomorphine. We quantified the response decay as the ratio between the firing rate 200 ms after the peak and the maximum firing rate (see Methods). Four clusters showed a change in response decay with apomorphine, with clusters #3, #5 and #15 revealing a faster decay to the full-field stimulus and cluster #4 revealing a slower decay (Fig. 1F).

Cluster #1 provides an example for sustained On-RGCs that changed their centre-surround organisation with apomorphine (Fig. 1D-F, Fig. 2A-C). Apomorphine reduced the maximum firing rate during the On response to the full-field spots (Fig. 2A,C; 103.8 ± 40.0 (before apomorphine, 'pre') vs. 89.9 ± 45.3 (with apomorphine, 'apo') spikes/s (mean \pm SD, $1200 \mu\text{m}$, $p=0.005$)), suggesting a strengthened surround. The maximum firing rates during the small square stimuli were also reduced (Fig. 2A-B, 107.0 ± 54.5 vs. to 89.6 ± 49.7 spikes/s ($150 \mu\text{m}$, $p<0.0001$), mean \pm SD). Apomorphine did not significantly change the response decay of this cluster (see Supporting Information). Here and in the following examples, effects of apomorphine were only partially washed out (after 30 mins), probably due to long-lasting effects such as on gap-junction phosphorylation (Bloomfield & Völgyi 2009, Goel & Mangel 2021, Roy & Field 2019).

In another cluster of non-direction selective On-Off RGCs (Cluster #4, Fig. 1C, Fig. 2D-F) we found the opposite effect. Here, the surround was weakened with apomorphine. RGCs in this cluster

displayed an increased firing rate to full-field stimuli with apomorphine in the On and Off response, as well as increased responses to the 75 μm square stimulus (Fig. 2D-F, 34.4 ± 15.9 vs. to 49.8 ± 22.3 spikes/s (1200 μm , On response, $p=0.006$); 27.6 ± 18.6 vs. 50.0 ± 29.0 spikes/s (1200 μm , Off response, $p<0.0001$); 58.8 ± 32.1 vs. 87.1 ± 56.2 spikes/s (75 μm , On response, $p=0.006$); 43.1 ± 32.2 vs. 59.7 ± 43.9 spikes/s (75 μm , Off response, $p=0.031$); mean \pm SD; see Supporting Information). RGCs in this cluster also showed a change in their response kinetics with apomorphine, which was stimulus-size dependent. Specifically, responses to the disappearance of a small square (Off response) became more transient, whereas those to a full-field stimulus became more sustained (0.44 ± 0.24 vs. 0.21 ± 0.26 fraction of peak response (75 μm , Off response, $p=0.025$); 0.21 ± 0.22 vs. 0.36 ± 0.29 (1200 μm , Off response, $p=0.043$); mean \pm SD; see Supporting Information).

Finally, we observed a more complex phenomenon in cluster #15, where apomorphine enhanced responses to small stimuli but did not significantly change responses to full-field stimuli (Fig. 2G-I, 74.1 ± 31.8 vs. 85.8 ± 35.5 spikes/s (150 μm , Off response, $p=0.015$); 88.6 ± 22.0 vs. 89.1 ± 34.7 spikes/s (1200 μm , Off response, $p=0.919$); mean \pm SD; see Supporting Information), suggesting an enhanced centre response. With apomorphine, responses of these RGCs became more transient (Fig. 2I (bottom), 0.41 ± 0.18 vs. 0.28 ± 0.14 fraction of peak (1200 μm , Off response, $p=0.0003$); mean \pm SD). Based on their responses, we suspected that this cluster may correspond to cluster 8b from (Baden et al. 2016), the tOff- α RGCs. Overall, our findings suggest that dopamine can have a multitude of effects on RGC receptive field organisation, and can also influence their response kinetics.

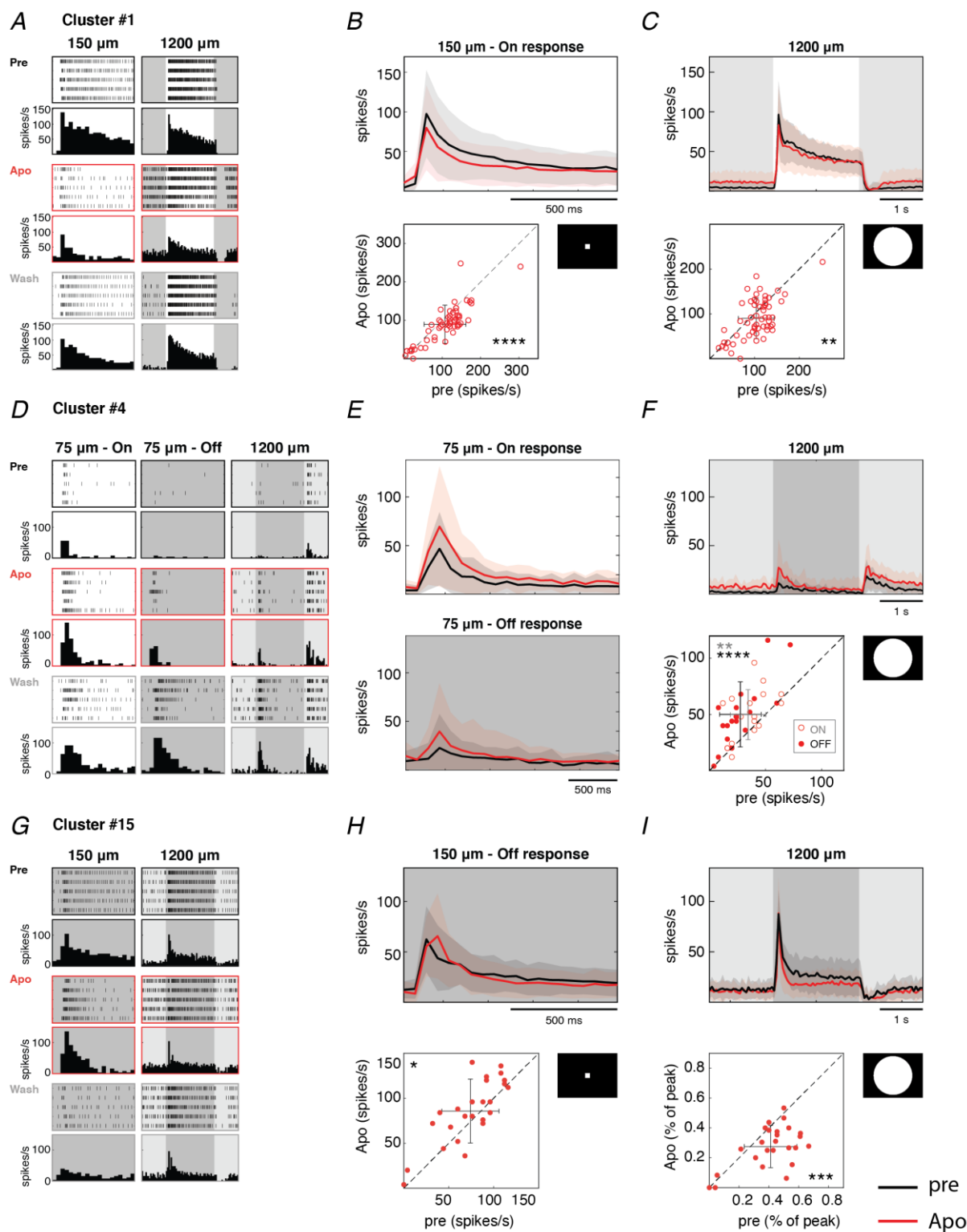


Figure 2. Apomorphine differentially affects responses to large vs. small stimuli in a subtype-specific manner. **A** Raster plot and mean PSTH of an example cell from cluster #1 (On cells) in response to

This article is protected by copyright. All rights reserved.

the onset of a 150 μm square and a full-field stimulus (1200 μm) in pre condition (black frame), with apomorphine (red frame) and after washout (grey frame). **B** Top: Mean \pm SD PSTHs of all cells of cluster #1 (n=57) in pre (black) and apomorphine (red) conditions in response to a small stimulus. Bottom: Maximum firing rate in response to the onset of the 150 μm square in pre condition (x-axis) and with apomorphine (y-axis) for all cells from this cluster. **C** Like B for the full-field response. **D** Like (A) for an example cell from cluster #4 (On-Off cells), showing the On and Off responses (white and grey background, respectively) to a 75 and 1200 μm stimulus. **E** Mean \pm SD PSTH of On (top, white background) and Off (bottom, grey background) responses to a 75 μm spot for all cells from cluster #4 (n=18 cells). **F** Like (C) with maximum firing rate during On and Off responses depicted by open and closed circles, respectively. **G** Like (A) for the Off responses of cluster #15 (Off cells, n=25 cells). **H** Top: Mean \pm SD PSTH of Off responses to a 150 μm square offset. Bottom: Maximum firing rate in response to offset of the square. **I** Top: Mean \pm SD PSTH in response to 1200 μm stimulus. Bottom: Comparison of response kinetics (fraction of response 200 ms after peak) of Off response of the 1200 μm stimulus in pre condition (x-axis) and with apomorphine (y-axis). For population analysis, individual dots represent single cells. Mean \pm SD are indicated in scatter plots. For **B**, **C**, **E**, **F**, **H**, **I**, asterisks above the unity line indicate increases with apomorphine and asterisks below indicate decreases. Colours of mean PSTHs as in the legend (bottom right). * $p < 0.05$, ** $p < 0.01$, *** $p < 0.001$, **** $p < 0.0001$ according to Wilcoxon signed rank test.

Apomorphine facilitates tOff- α RGC light responses to small spot stimuli

Since we suspected that cluster #15 (Fig. 2G-I) corresponds to the well-studied tOff- α RGC (Krieger et al. 2017, Manookin et al. 2008, Münch et al. 2009, Murphy & Rieke 2008, Pang et al. 2003, Wang et al. 2021, Warwick et al. 2018) we set to gain a deeper understanding of how the dopamine receptor agonist apomorphine affects the centre-surround organisation of this RGC subtype. To this end, we conducted two-photon targeted patch clamp recordings of tOff- α RGCs labelled in the Calb2-EGFP transgenic mouse line (Huberman et al. 2008). To match our MEA experiments, and because we previously reported different activity patterns in the dorsal and ventral retina (Warwick et al. 2018), we exclusively recorded from cells in the dorsal retina. The light stimulus consisted of a dark spot centred on the cell soma, appearing for 2 s on a grey background. In order to examine the receptive

field properties, we used a variety of spot sizes, ranging from 50 to 800 μm in diameter (Fig. 3A; see Methods).

To start with, we characterised the light responses of tOff- αRGCs under control conditions (Fig. 3B). These cells displayed an Off response to the dark spots and had a peak maximum firing rate to the 300 μm spot, after which the maximum firing rate decreased for increasing spot size. This decrease is mediated by surround antagonism, which is known to be weak but apparent in tOff- αRGCs (Farrow et al. 2013, Warwick et al. 2018). Like for the MEA data, we quantified the surround antagonism using the SSI ((Hoggarth et al. 2015); see Methods). Control tOff- αRGCs had an SSI of 0.19 ± 0.11 (mean \pm SD) due to their weak antagonistic surrounds. Next, we repeated the experiments in the presence of apomorphine (10 μM) to mimic the effect of increasing dopamine levels in the retina (Fig. 3C). Apomorphine did not increase the surround antagonism (SSI of 0.19 ± 0.11 (pre) vs. 0.17 ± 0.07 (apo), $p=0.518$). However, similarly to the effects on cluster #15, the dopamine receptor agonist did facilitate tOff- αRGC responses, significantly increasing their maximum firing rates to the smallest spot sizes (50-200 μm spots; Fig. 3C-E). Moreover, apomorphine tended to shorten the responses of tOff- αRGCs , and this was significant for the smallest spot sizes (50-200 μm spots; Fig. 3F). These findings suggest that dopamine can enhance centre-mediated responses in tOff- αRGCs and change their response kinetics.

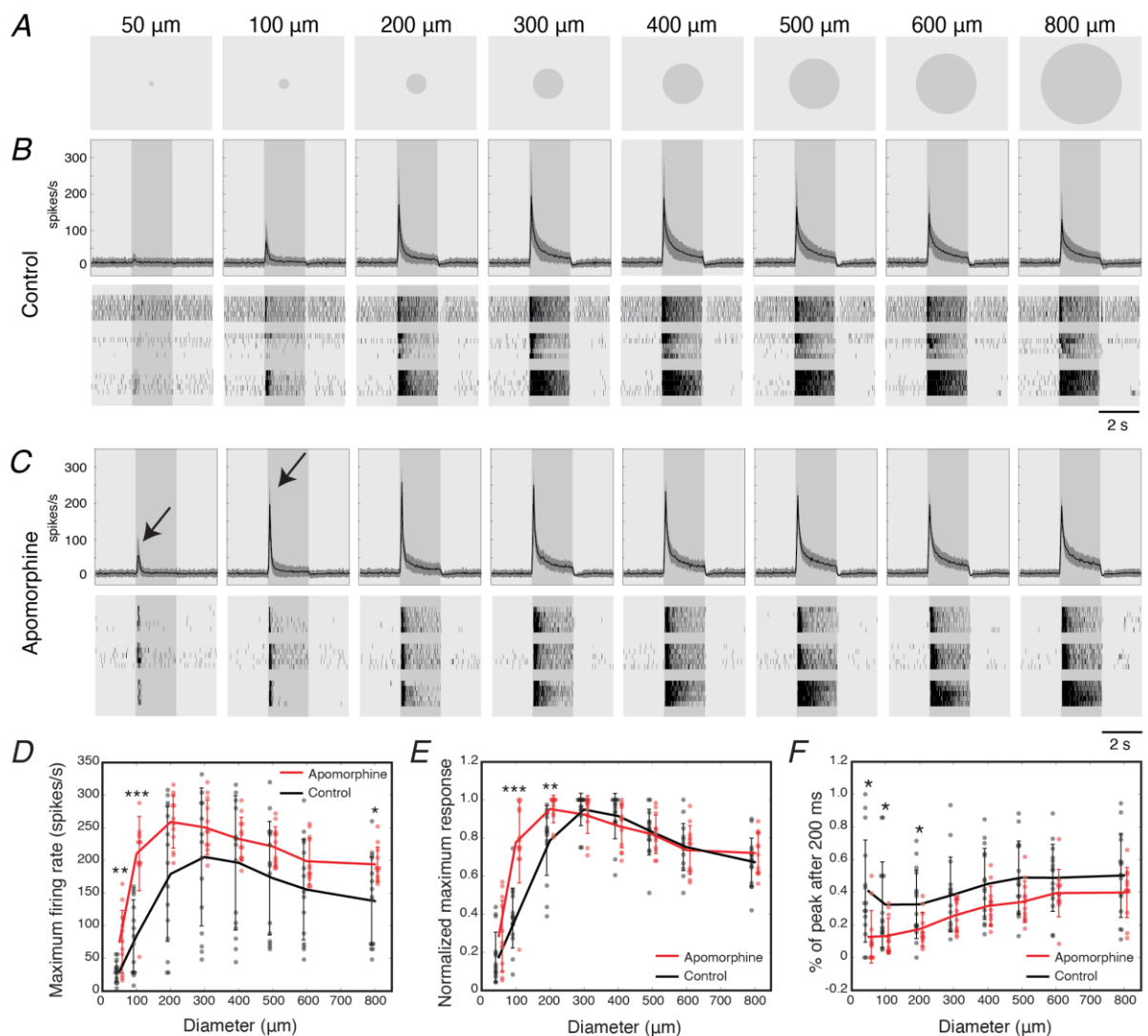


Figure 3. Apomorphine does not enhance surround antagonism but increases firing rates of tOff-αRGCs in response to small spot stimuli. **A** Diagram illustrating the different sized spots used as light stimuli. **B-C** Top: Mean ± SD firing rate of tOff-αRGCs under control conditions (**B**) and in the presence of apomorphine (10 μM) (**C**). Arrows indicate increased response to small spot stimuli with apomorphine. Bottom: Raster plots of three example tOff-αRGCs. Each row corresponds to 5 repeats of the stimulus. **D** Maximum firing rate (spikes/s) as a function of spot size for control tOff-αRGCs (black) and tOff-αRGCs in the presence of apomorphine (red). **E** Normalised maximum response as a function of spot size for control tOff-αRGCs (black) and tOff-αRGCs in the presence of apomorphine (red). **F** Response decay quantified as the fraction of the maximum firing rate 200 ms after the peak. n=15 tOff-αRGCs from 15 mice for control conditions, n=12 tOff-αRGCs from 5 mice in the presence of apomorphine. For D-F, dots represent single cells. Error bars represent the mean ± SD. Dots and

error bars were offset/jittered for legibility. * $p < 0.05$, ** $p < 0.01$ and *** $p < 0.001$ according to Wilcoxon rank-sum test.

In order to investigate how reduced levels of dopamine affect the receptive field properties of tOff- α RGCs, we used dopamine receptor antagonists (Fig. 4). Raclopride (2.5 μ M) was used to inhibit D₂-R and SCH-23390 (1 μ M) was used to inhibit D₁-R. Under D₂-R blockade, surround antagonism was abolished (SSI of 0.19 ± 0.11 (pre) vs. -0.01 ± 0.20 (D₂-R block), $p=0.008$). No significant difference was observed between the SSI of tOff- α RGCs under control conditions and blockade of D₁-R (0.19 ± 0.11 vs. 0.06 ± 0.28 , $p=0.098$). However, antagonists for both D₂-R and D₁-R reduced Off responses to the smaller spot sizes (Fig. 4B-E). Blockade of D₂-R significantly reduced the maximum firing rates of tOff- α RGCs in response to the 200 and 300 μ m spots (Fig. 4D), and blockade of D₁-R significantly reduced the maximum firing rates in response to the 200-500 μ m spots (Fig. 4E).

As apomorphine affected the firing rates of tOff- α RGCs, we normalised each individual tOff- α RGC to its overall maximum firing rate in order to compare receptive field shape between the different groups (Figs. 3E, 4F). Under control conditions, tOff- α RGCs responded maximally to the 300 μ m spot. The dopamine receptor agonist apomorphine shifted the maximum response to a smaller spot size of 200 μ m (Fig. 3E), whereas the D₂-R and D₁-R antagonists shifted it to larger spots of 600 and 500 μ m, respectively (Fig. 4F). These data suggest that dopamine may affect the receptive field organisation of tOff- α RGCs by increasing the centre Off response to smaller stimuli.

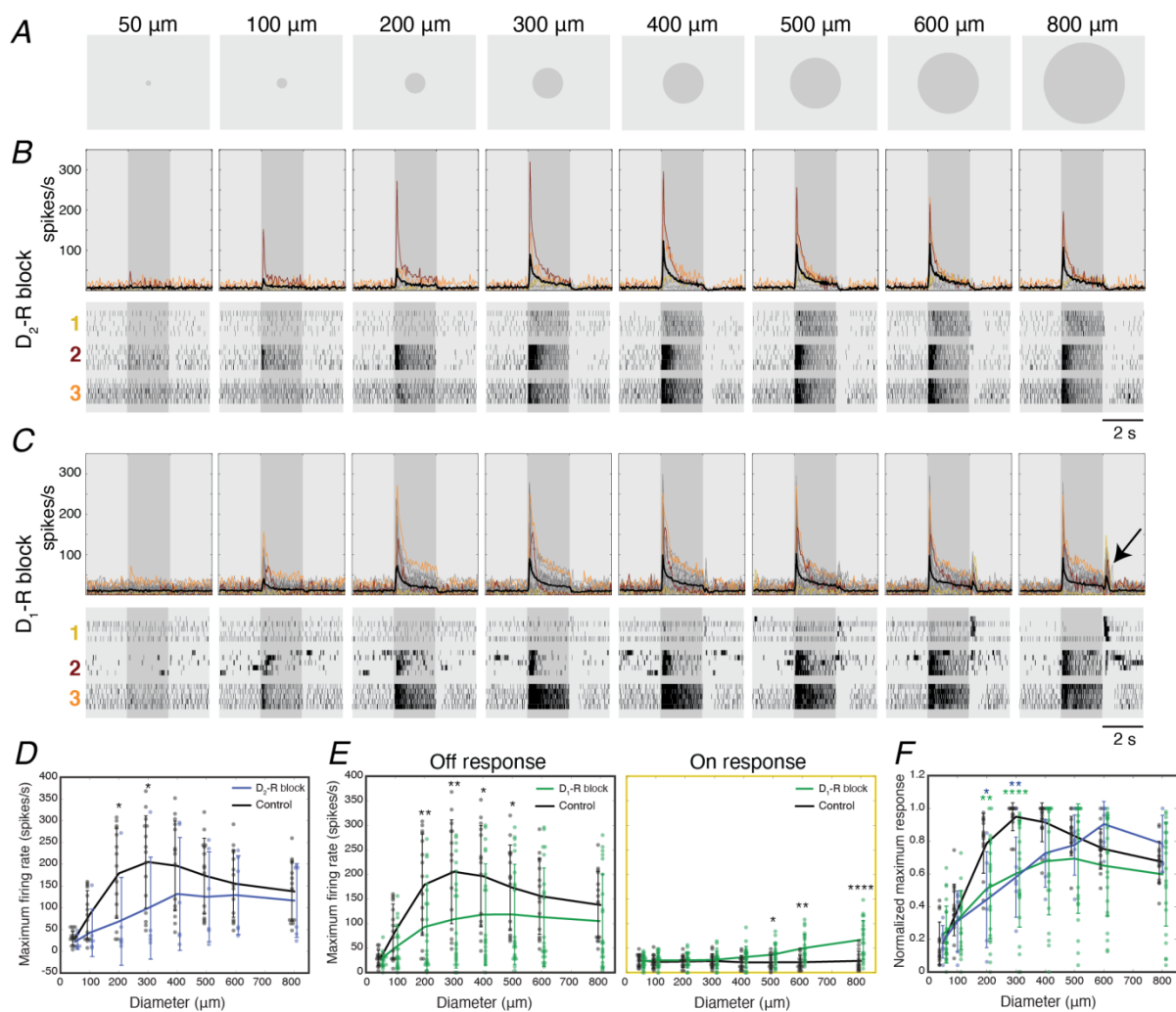


Figure 4. Blockade of both D_2 -R and D_1 -R reduces Off responses to small spot stimuli, but only D_1 -R blockade causes On responses to large spot stimuli. **A** Diagram illustrating the different sized spots used as light stimuli. **B-C** Firing rate and raster plots of tOff- α RGCs under blockade of D_2 -R (**B**) and D_1 -R (**C**). Individual PSTHs are shown in grey, except for the three examples shown in the raster plots below, which are indicated by the numbers on the left. Mean PSTH is overlaid in black. Arrow indicates surround-activation On response with D_1 -R blocker. For (**C**), the example raster plots display two extreme cases of a cell with diminished Off response (cell 1) and a cell with no On response (cell 3), together with a representative cell, which maintained its Off response alongside revealing an On response (cell 2). **D** Maximum firing rate (spikes/s) as a function of spot size for control tOff- α RGCs (black) and tOff- α RGCs under D_2 -R blockade (**D**, blue). **E** Maximum firing rate (spikes/s) for the Off (left) and On (right) responses as a function of spot size for control tOff- α RGCs (black) and under D_1 -R blockade (green). **F** Normalised maximum Off response as a function of spot size for control tOff- α RGCs (black line), tOff- α RGCs under D_2 -R (blue line) and D_1 -R blockade (green line). Colours match **D-E**. $n=15$ tOff- α RGCs from 15 mice for control conditions, $n=6$ tOff- α RGCs from

This article is protected by copyright. All rights reserved.

6 mice for D₂-R blockade, n=22 tOff-αRGCs from 16 mice for D₁-R blockade. For *D-F*, dots represent single cells. Dots were jittered for legibility. Error bars represent the mean±SD, * $p < 0.05$, ** $p < 0.01$ and **** $p < 0.0001$ according to Wilcoxon rank-sum test.

D₁-R blockade reveals On responses in tOff-αRGCs

We recorded from a total number of 22 tOff-αRGCs under D₁-R blockade. Interestingly, they did not only change their Off responses under this condition. Examination of their responses revealed a transient On response to the disappearance of the larger dark spots, most notably the 800 μm spot (Fig. 4C). The maximum firing rates during light onset (2 s following the dark spot disappearance) revealed that this On response emerged for the spots sized 500-800 μm compared with control tOff-αRGCs (Fig. 4E, right). In total, 16 out of 22 tOff-αRGCs displayed a significant increase in firing rate after the disappearance of the black spot. We observed some variability in the responses of tOff-αRGCs under D₁-R blockade (Fig 4C) that may be due to differences in the underlying circuits, which vary with location along the ventral-dorsal retinal axis in a gradual manner (Warwick et al., 2018). Another possible source of variability can be different drug incubation times (see Discussion).

Some cells that exhibited On responses had decreased or even absent Off responses (Fig. 4C). Comparing control tOff-αRGCs to the tOff-αRGCs subpopulation that exhibited On responses under D₁-R blockade revealed a significant decrease in the Off response duration to the 800 μm spot from 1287±581 to 538±720 ms (mean±SD, $p=0.004$). For the 6/22 cells that did not exhibit On responses, we observed no decrease in Off response duration to the 800 μm spot (1808±139 ms). This suggests that the On and Off responses are mediated by opposing mechanisms. As opposed to the Off response, which decreased to the smaller spot stimuli, the On response under D₁-R blockade emerged at large stimuli (500 μm) and increased with spot size (Fig. 4E, right), suggesting that these

On responses resulted from surround activation. We next aimed at revealing the source for these On responses in tOff- α RGCs.

The tOff- α RGC is known to receive synaptic input from both the Off and On pathways. While the tOff- α RGC receives glutamatergic (excitatory) input from the Off pathway via Off cone bipolar cells and potentially from vGlut3 amacrine cells (Kim et al. 2020, Lee et al. 2016), it also receives glycinergic (inhibitory) input from the On pathway via All amacrine cells. These All amacrine cells depolarize during light onset as they are excited by rod bipolar cells (forming the primary rod pathway; (Murphy & Rieke 2008, van Wyk et al. 2009) and are gap-junction coupled to On cone bipolar cells (Fig. 5A) (Beaudoin et al. 2008, Demb & Singer 2012, Manookin et al. 2008, Münch et al. 2009, Murphy & Rieke 2006). As a result, tOff- α RGCs are activated during light offset in a push-pull mechanism, excited by Off bipolar cells (via the Off pathway) and at the same time disinhibited by All amacrine cells (via the On pathway) (Manookin et al. 2008, van Wyk et al. 2009). Previously, it was thought that rods are saturated at photopic light levels and do not contribute to the processing of light information under high illumination conditions. However, recent work has shown that this is not the case (Szikra et al. 2014, Tikidji-Hamburyan et al. 2017, Vlasits et al. 2014), leading us to speculate that the On responses we detected in tOff- α RGCs could arise from the primary rod pathway.

To establish whether the On pathway was indeed responsible for the On responses detected in tOff- α RGCs in the presence of D₁-R blockade, we selectively blocked the On pathway by adding L-AP4 (5 μ M), a selective group III metabotropic glutamate receptor agonist, to the Ames solution (Fig. 5B). None of the 5/5 tOff- α RGCs examined displayed an On response to large spots in the presence of a D₁-R-antagonist and L-AP4 (Fig. 5C-G), confirming that the On pathway was responsible for the observed On responses in tOff- α RGCs during D₁-R blockade. Two other observations were made

This article is protected by copyright. All rights reserved.

during L-AP4 application. Firstly, the combination of the D₁-R antagonist + L-AP4 increased the background firing activity compared to the D₁-R antagonist alone from 8.5 ± 8.6 to 36.7 ± 24.4 spikes/s (mean \pm SD, $p=0.041$; Fig. 5D-G). Under control conditions, tOff- α RGCs are known to receive tonic inhibition from All amacrine cells (Manookin et al. 2008). Although the increase in background activity in the presence of D₁-R antagonist + L-AP4 may suggest that tonic inhibition exists under D₁-R antagonist alone, whether this is indeed the case is not known. Note that the high background activity observed under D₁-R antagonist + L-AP4 is responsible for the relatively high firing rates during light onset in Fig. 5G (yellow line), which does not correspond to actual light responses. Secondly, tOff- α RGCs had higher maximum firing rates to the appearance of the dark spot (light offset) in the presence of the D₁-R-antagonist + L-AP4 compared to the D₁-R-antagonist alone (Fig. 5H). L-AP4 alone is expected to decrease Off responses in tOff- α RGCs via the loss of the 'push-pull' mechanism (Manookin et al. 2008). Our results suggest that D₁-R blockade compensates for this decrease, either via enhancing tOff- α RGCs Off-pathway input or via another unknown pathway.

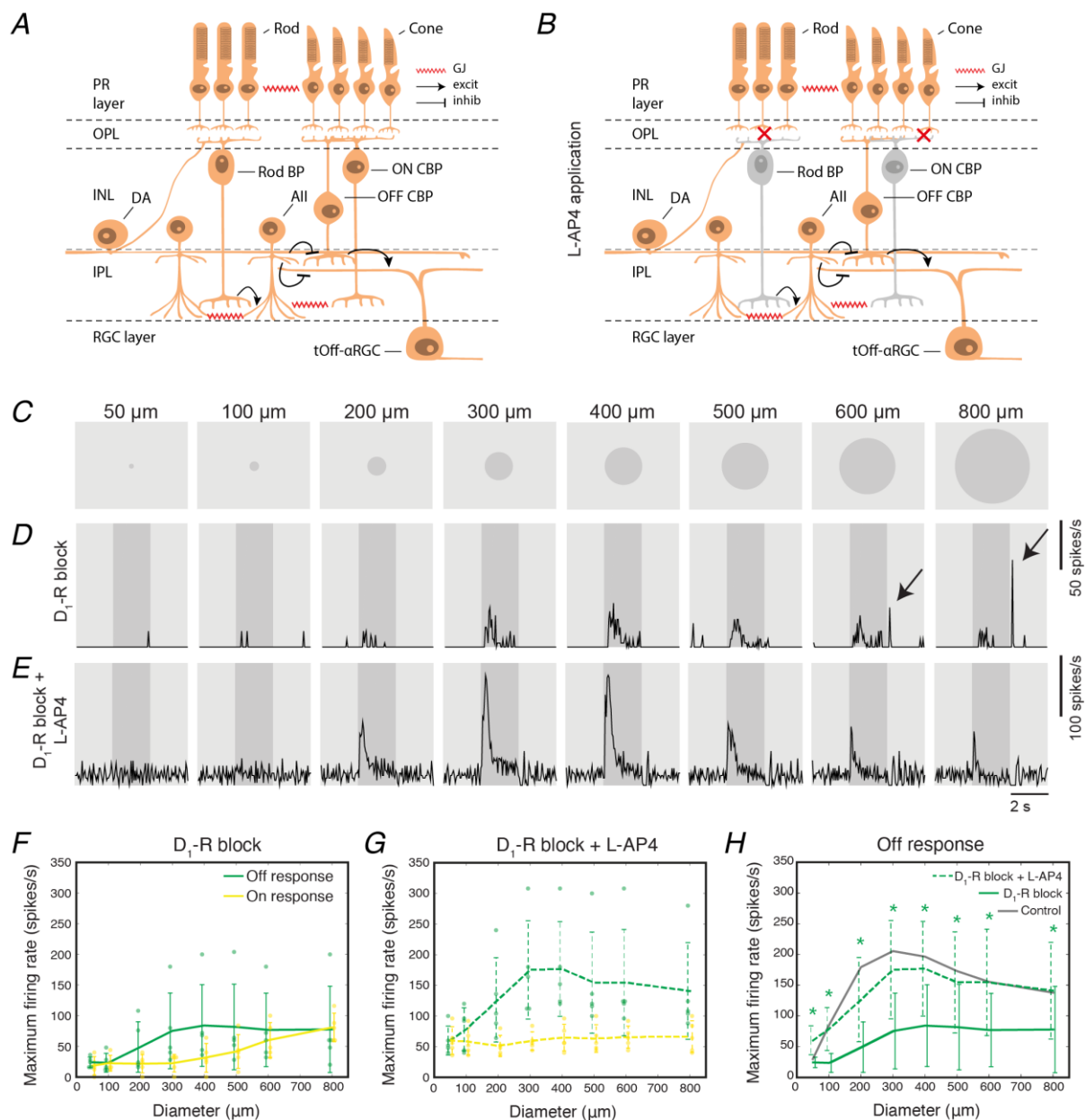


Figure 5. The On pathway mediates On responses in tOff-αRGCs under D_1 -R blockade. **A** Diagram illustrating the main pathways underlying the response in tOff-αRGCs. PR, photoreceptor; OPL, outer plexiform layer; INL, inner nuclear layer; IPL, inner plexiform layer; BP, bipolar; CBP, cone bipolar; DA, dopaminergic amacrine cell; GJ, gap junction; excit, excitation; inhib, inhibition. **B** Same as in (A) except after L-AP4 application. **C** Diagram illustrating the different sized spots used as light stimuli. **D-E** Mean firing rate of an example tOff-αRGC under D_1 -R blockade (D) and after addition of L-AP4 (E). On responses (indicated by arrows) disappeared with L-AP4. **F-G** Maximum On (yellow) and Off (green) firing rates as a function of spot size under D_1 -R blockade prior to addition of L-AP4 (F) and

This article is protected by copyright. All rights reserved.

following addition of L-AP4 (5 μ M) (G). **H** Maximum Off firing rates as a function of spot size for the 5 tOff- α RGCs before and after the addition of L-AP4 while under D₁-R blockade. Maximum firing rates under control conditions are shown for comparison (black). Control (black) is taken from Fig. 3 and 4 for comparison. Asterisks indicate significant difference between D₁-R blockade before and after addition of L-AP4. n=5 tOff- α RGCs from 4 mice for D₁-R blockade and after the addition of L-AP4. n=15 tOff- α RGCs from 15 mice for control conditions. For F-H, dots represent single cells. Dots were jittered for legibility. Error bars represent mean \pm SD, * $p < 0.05$ according to Wilcoxon signed rank test.

D₁-R blockade has differential effects on the multiple pathways underlying the tOff- α RGC response

In order to establish how the different circuits underlying the tOff- α RGC response are affected under D₁-R blockade, we conducted whole-cell voltage-clamp recordings (Fig. 6). Voltage-clamping the tOff- α RGC at 0 mV and -60 mV allowed us to separate the inhibitory and excitatory inputs, respectively. The All amacrine cell is considered the main inhibitory presynaptic partner to the tOff- α RGC, however, other inhibitory cells may contribute. Off cone bipolar cells are considered the main excitatory presynaptic partners to the tOff- α RGC. Note that All amacrine cells can also influence the glutamatergic input onto the tOff- α RGC by forming glycinergic synapses onto the Off cone bipolar cells (Fig. 5A) (Manookin et al. 2008, Murphy & Rieke 2008, Warwick et al. 2018).

Examining the excitatory input to tOff- α RGCs under control conditions revealed a transient and a sustained component during light offset (Fig. 6B). The transient component, which is thought to originate from cone pathways (Warwick et al. 2018), peaked in response to the 200 μ m spot and disappeared entirely for the 800 μ m spot, suggesting it is susceptible to strong surround antagonism. This is in contrast to D₁-R blockade where the transient excitation peaked at the 400 μ m spot and was still present in response to the 800 μ m spot, suggesting weaker surround antagonism (Fig. 6C, D). The maximum excitatory currents were significantly reduced for the 50-300 μ m spots under D₁-R

blockade (Fig. 6D). This reduction in excitation could contribute to the lower firing rates observed during the extracellular recordings (Fig. 4E).

The sustained excitatory component present under control conditions is likely the result of All glycinergic synapses onto the terminals of Off cone bipolar cells (Fig. 6B). Under D_1 -R blockade, the sustained excitatory component is greatly diminished (Fig. 6C), suggesting a loss of input from All amacrine cells to Off cone bipolar cells.

Examining the inhibitory input to tOff- α RGCs under control conditions revealed a strong sustained disinhibition at light offset that showed weak surround antagonism (Fig. 6B, E) (Warwick et al. 2018). This disinhibition largely originates from All amacrine cells, although other inhibitory cells may contribute (Manookin et al. 2008, Warwick et al. 2018). Under D_1 -R blockade, disinhibition was greatly diminished for smaller spot sizes (in accordance with the diminished sustained excitation) and a gain of inhibition was observed for larger spot sizes (Fig. 6C, E). Consequently, disinhibition at light onset (following the disappearance of the dark spot) was observed for large spots (Fig 6C), which could underlie the On responses observed in the spiking activity of tOff- α RGCs under D_1 -R blockade (Fig. 4C, E). Additionally, this change from disinhibition to inhibition at light offset may explain why tOff- α RGCs with On responses reduced their sustained Off responses.

Under control conditions All amacrine cells are thought to provide tonic inhibition to the tOff- α RGC that is then released at light offset (Manookin et al. 2008). The lack of disinhibition at light offset under D_1 -R blockade suggests a loss of input from All amacrine cells to the tOff- α RGC, in line with the loss of the sustained excitation that is also thought to be mediated via All cells. Comparing the injected current needed to hold the cell at 0 mV revealed a significant decrease for tOff- α RGCs under D_1 -R blockade (Fig. 6F). This could be the result of a more depolarised resting potential in the

presence of the D₁-R antagonist, and/or increased input resistance due to loss of tonic inhibitory conductance. Indeed, we found that the input resistance was increased from 48.9±7.2 mΩ to 98.5±65.1 mΩ (mean±SD) with the D₁-R antagonist ($p = 0.032$, Wilcoxon rank-sum test). Either way, our observation of reduced holding current could be caused by the loss of tonic inhibition from All amacrine cells. While a loss of input from All amacrine cells can explain the loss of disinhibition at light offset, it does not explain the gain of inhibition for large spot sizes. One possibility is that this gain of inhibition was previously masked by the strong disinhibition. Another possibility is that D₁-R blockade caused the tOff-αRGC to gain an additional inhibitory input in its surround receptive field (see Discussion).

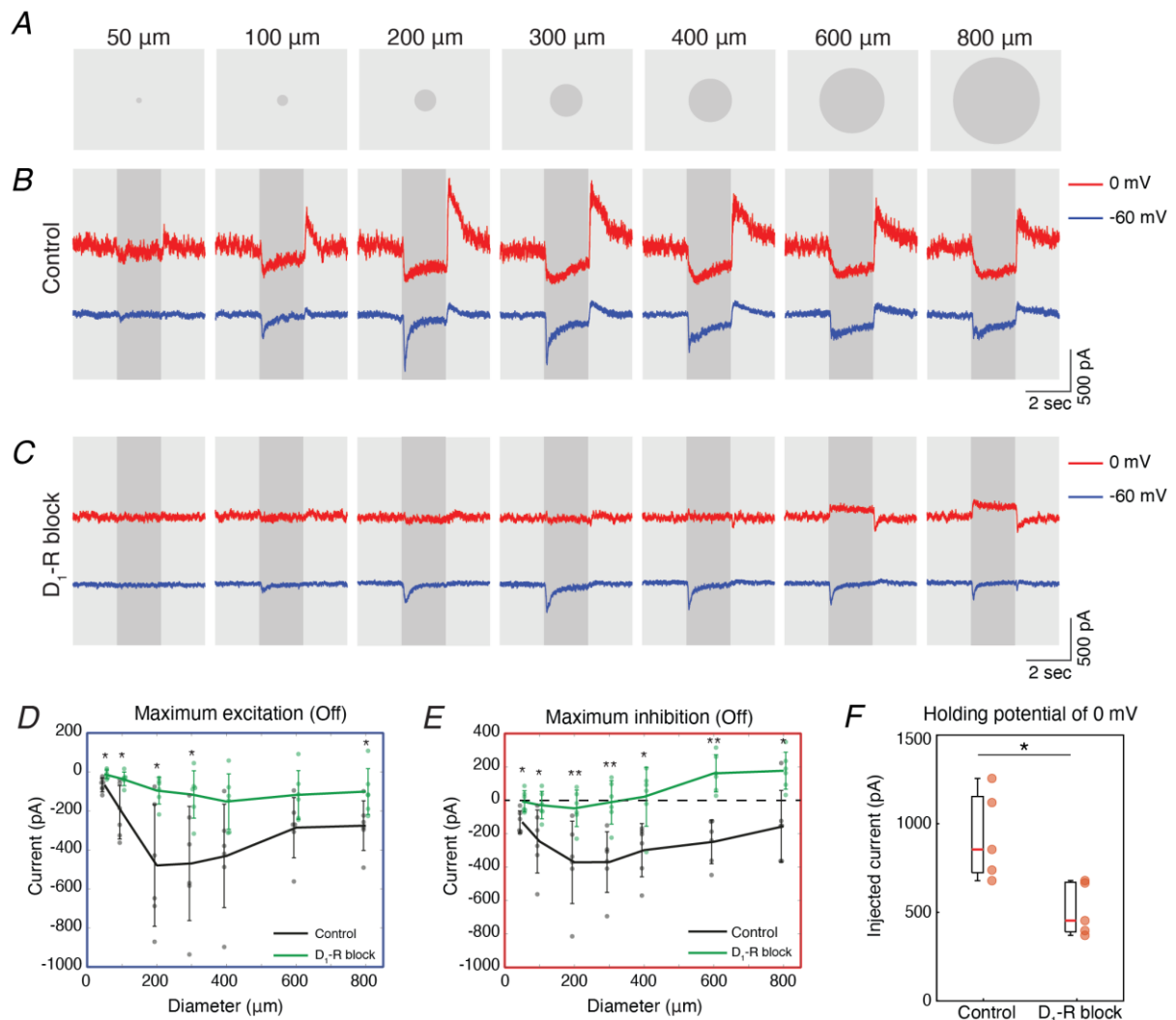


Figure 6. *D*₁-R blockade differentially affects the inhibitory and excitatory inputs onto the tOff- α RGC. **A** Diagram illustrating the different sized spots used as light stimuli. **B-C** Current traces of an example control tOff- α RGC (**B**) and an example tOff- α RGC under *D*₁-R blockade (**C**) when held at 0 (red) and -60 (blue) mV. **D** Maximum excitatory current during Off stimulus as a function of spot size for control tOff- α RGCs (black line) and tOff- α RGC under *D*₁-R blockade (green line). **E** Same as (**D**) Maximum for inhibitory current. **F** Box plots and data points for the injected current needed to hold the cell at 0 mV from the resting potential during the presentation of the grey background for control tOff- α RGCs and tOff- α RGCs under *D*₁-R blockade. For **D-E**, $n = 6$ tOff- α RGCs. For **F**, $n=5$ tOff- α RGCs from 5 mice for control conditions, $n=5$ tOff- α RGCs from 3 mice for *D*₁-R blockade. For **D-F**, dots represent single cells. Dots were jittered for legibility. Error bars represent the mean \pm SD, * $p < 0.05$ and ** $p < 0.01$ according to Wilcoxon rank-sum test.

Thus, D₁-R blockade had specific effects on the different synaptic components arriving onto the tOff- α RGC. Firstly, it reduced transient excitatory inputs derived from Off cone bipolar cells and weakened their surround antagonism. Secondly, it reduced inputs from the primary rod pathway and caused an increase in inhibition to occur at light offset for larger spot sizes, resulting in surround activation of tOff- α RGCs. In conclusion, dopamine appeared to affect distinct retinal pathways differently, and its role in shaping RGCs' centre-surround receptive fields is specific to individual RGC subtypes and the pathways underlying their responses.

Discussion

In this study we sought to investigate how dopamine shapes the receptive field properties of RGCs. We first show, using MEA recordings, that a dopamine receptor agonist can both strengthen or weaken an RGC's surround and does so in a subtype-specific manner. We then proceeded to study a specific genetically labelled RGC subtype, the tOff- α RGC. We observed that the dopamine receptor agonist apomorphine facilitates light responses to small stimuli, whereas dopamine receptor antagonists reduce them. Blockade of D₁-R revealed responses of opposite polarity (On responses) in response to large stimuli, characteristic of surround activation. Using voltage-clamp recordings, we showed that while D₁-R blockade weakened the surround of excitatory inputs, it enhanced the surround of inhibitory inputs, leading to disinhibition at light onset for large spot stimuli, which underlie the On response. Together, these data suggest that the role of dopamine in shaping receptive field properties of RGCs results from its specific effects on distinct retinal pathways.

This article is protected by copyright. All rights reserved.

Combining population and single-cell recordings to uncover subtype-specific effects of dopamine

Dopamine has long been reported to increase surround inhibition of RGCs (Jensen 1991; Jensen & Daw 1984, 1986). However, dopamine's effects on RGCs' receptive fields are likely to be far more complicated given what we know about its multiple functions, including modulating gap junctions and altering intrinsic cellular conductances (Bloomfield & Völgyi 2009, Goel & Mangel 2021, Roy & Field 2019). The picture is further complicated by the fact that dopamine receptors are expressed on every major cell type of the retina, including RGCs themselves, and that these receptors can be divided into two families that may have opposing effects (Witkovsky 2004).

Using MEA recordings and clustering, we were able to group RGCs into functional subtypes. While we likely underestimated the number of subtypes, we did identify changes to receptive field structure that are consistent within clusters, which correspond to one or possibly multiple yet very similar RGC subtypes. Recording from hundreds of RGCs simultaneously, we could not optimally stimulate each RGC at its receptive field centre. Thus, for many cells the 'centre' stimulus may be slightly offset from the cell's receptive field centre (see example in Fig. 1B, bottom left) and therefore not elicit the optimal response. Moreover, non-linear dendritic integration can add to response variability, depending on the location of the stimulus on the cell's receptive field (Enroth-Cugell & Robson 1966, Grimes et al. 2014, Ran et al. 2020). Using patch clamp recordings, we were then able to display a greater number of stimulus sizes that were exactly centred on the recorded cell, as well as use a contrast that elicited optimal responses for tOff- α RGCs (black spot on grey background; (Warwick et al. 2018)). These differences in the light stimuli may underlie some variability between MEA and patch clamp experiments. Importantly, our finding from the MEA

recordings – enhanced responses to small stimuli with apomorphine – match those of tOff- α RGC targeted recordings, suggesting that cluster #15, the ‘tOff- α cluster’, either exclusively contains tOff- α RGCs, or at least that a large proportion are tOff- α RGCs. Our results show that the approach of large-scale population recordings, subsequent clustering of cells and targeting of known subtypes for detailed electrophysiological experiments can yield detailed results about underlying circuits.

Mechanisms of D_1 -R and D_2 -R activation in shaping tOff- α RGC responses

Despite D_1 -R and D_2 -R having opposing effects, we found some similarity between the effects of D_1 -R and D_2 -R blockers, as both reduced Off responses in tOff- α RGCs to small spot stimuli. Accordingly, apomorphine increased tOff- α RGC responses to small spot stimuli. Previously, dopamine was shown to enhance glutamate-gated currents in Off cone bipolar cells of the salamander retina via D_1 -R (Maguire & Werblin 1994). If the same mechanism exists in the mouse retina, this could explain the increased responses of tOff- α RGCs to small stimuli in the presence of the dopamine receptor agonist as well as the decreased responses under D_1 -R blockade. However, another mechanism must be responsible for reducing responses to small spot stimuli during D_2 -R blockade. Heterotypic gap-junctional coupling between rods and cones is regulated by dopamine via D_2 -R, specifically the D_4 receptor (Li et al. 2013, Ribelayga et al. 2008). Blocking this receptor causes an increase in gap-junctional coupling between rods and cones (Bloomfield & Völgyi 2009, Roy & Field 2019) that will lower the photoreceptors’ input resistance and may therefore weaken the signal that is transduced to bipolar cells. It may also weaken the antagonistic surround of the photoreceptors, which in turn affects the antagonistic surround of bipolar cells. This provides a

This article is protected by copyright. All rights reserved.

potential explanation for the decrease in responses of tOff- α RGCs to small spot stimuli and loss of surround antagonism under D₂-R blockade.

A difference observed between D₁-R and D₂-R blockade was that only D₁-R blockade caused surround activation, as was evident by the On responses in tOff- α RGCs to large spot stimuli. Pharmacological blockade of the On pathway indicated that these On responses originate from the On pathway. Voltage-clamp experiments suggested that they were mediated by changes in inhibition, as under D₁-R blockade tOff- α RGCs exhibited inhibition at light offset and disinhibition at light onset for larger spot sizes.

Examining a dataset of single-cell RNA transcriptomics data revealed that tOff- α RGCs express *drd1* – the gene coding for the D₁-R receptor (Single Cell Portal (SCP), Broad Institute, based on (Tran et al. 2019)). This suggests the effects we detected with apomorphine and the D₁-R antagonist result (at least partly) from a direct activation of the tOff- α RGCs.

Variability in tOff- α RGC responses

Under D₁-R blockade, tOff- α RGC responses were quite variable, as the On response was observed in most, but not all, recorded cells, and the Off response tended to decrease only in these cells. This variability may originate from different locations of the recorded cells within the retina, since response properties of tOff- α RGC vary with their location along the ventral-dorsal retinal axis in a gradual manner (Heukamp et al. 2020, Warwick et al. 2018). Thus, although we only recorded from tOff- α RGCs located in the dorsal half of the retina, the circuits that underlie responses of tOff- α RGCs in the dorsal-most part and in the central part of the retina may differ.

This article is protected by copyright. All rights reserved.

Another possible source of variability can be the incubation times of the D₁-R blocker. Before recording we incubated the retina for 30 min in the D₁-R antagonist so that the long-term effects of D₁-R blockade, such as changes in gap-junctional coupling (Bloomfield & Völgyi 2009, Goel & Mangel 2021, Roy & Field 2019), could take effect. The time it took to patch each tOff-αRGC varied and on some occasions more than one tOff-αRGC was patched in each retina piece, resulting in some cells having longer incubations in the D₁-R antagonist. While dopamine acts in a paracrine fashion and could therefore be washed out in our experimental preparation, our results suggest that retinal dopamine levels are not zero as we did observe specific effects with dopamine receptor antagonists. We therefore assume that dopaminergic amacrine cells, like other retinal cells, remain active and continue to release dopamine in the *ex vivo* retinal preparation and that dopamine is not washed out.

Role of All cells and D₁-Rs in shaping tOff-αRGC responses

Several lines of evidence suggest that under D₁-R blockade the tOff-αRGC loses input from the All amacrine cell. Firstly, Off responses were reduced under D₁-R blockade compared with control conditions, but got stronger in the presence of L-AP4, which blocks the On pathway. This is in contrast to control conditions, where the On pathway is thought to enhance Off responses in tOff-αRGCs via All disinhibition, and therefore Off responses are expected to be reduced in the presence of L-AP4. Secondly, when examining voltage-clamp recordings under D₁-R blockade, we observed a loss of sustained disinhibition arriving at the tOff-αRGC, as well as a loss of a sustained excitation, which is thought to arise from All amacrine cell synapses onto Off cone bipolar cells. In accordance, when examining the spiking activity, the duration of the Off response is reduced in cells with On

responses during D_1 -R blockade compared with control tOff- α RGCs. Lastly, quantifying the current needed to hold the tOff- α RGC at 0 mV revealed a significant decrease under D_1 -R blockade, possibly due to a loss of tonic inhibition from All amacrine cells. All amacrine cells express D_1 receptors (Nguyen-Legros et al. 1997) and are gap-junction coupled among themselves (Bloomfield & Völgyi 2009). Could the loss of synaptic input from All amacrine cells be the result of altered gap-junctional coupling among All amacrine cells? All amacrine cell gap-junctional coupling is triphasic – low in starlight, high in twilight and low again in daylight (Bloomfield & Völgyi 2009). While it is clear that light adaptation is responsible for both increase in coupling from starlight to twilight and decrease in coupling from twilight to daylight, it is only decoupling at higher light levels that is thought to be mediated by dopamine (Roy & Field 2019). This suggests that blocking D_1 -R would increase All coupling, which may decrease their input resistance and therefore reduce their excitability and signalling onto tOff- α RGCs. In addition, since dopaminergic amacrine cells form perisomatic rings directly around All amacrine cells (Debertin et al. 2015), it is possible that under control conditions the activity of the All amacrine cells is enhanced by direct input from dopaminergic amacrine cells. Blocking D_1 -R would have the opposite effect, reducing All amacrine cell activity and consequently reducing input from All amacrine cells to tOff- α RGCs. However, this would still not explain the gain of inhibition observed for larger spot sizes. A possible explanation for this phenomenon is that a reduction in disinhibition uncovers an inhibitory signal that may or may not have been there under control conditions. We do know that this inhibitory input is mediated by the On pathway and is therefore likely to originate from an On amacrine cell.

Conclusion

This article is protected by copyright. All rights reserved.

Previously, dopamine was thought to have a similar influence on all RGCs, namely to enhance their surround to increase spatial sensitivity at high illumination. At low illumination, when dopamine levels are low, the surround is comparatively weak to enhance spatial averaging and sensitivity to weak inputs (Rivlin-Etzion et al. 2018). As opposed to this simplified view, our findings demonstrate that a dopamine receptor agonist affects the centre-surround organisation of RGC receptive fields in a subtype-specific manner, via the differential effects it has on retinal pathways. Recent work reveals that centre-surround organisation does not merely control spatial integration, but may also contribute to more complex functions, such as motion detection (Ankri et al. 2020, Strauss et al. 2022). Thus, the differential effects dopamine has on different RGC subtypes may intricately shape visual processing to accommodate the visual requirements at different environmental conditions.

Bibliography

- Ankri L, Ezra-Tsur E, Maimon SR, Kaushansky N, Rivlin-Etzion M. 2020. Antagonistic Center-Surround Mechanisms for Direction Selectivity in the Retina. *Cell Rep.* 31(5):107608
- Baden T, Berens P, Franke K, Román Rosón M, Bethge M, Euler T. 2016. The functional diversity of retinal ganglion cells in the mouse. *Nature.* 529(7586):345–50
- Barlow HB, Fitzhugh R, Kuffler SW. 1957. Change of organization in the receptive fields of the cat's retina during dark adaptation. *J. Physiol. (Lond.).* 137(3):338–54
- Bauer B, Ehinger B, Åberg L. 1980. [3H]-Dopamine release from the rabbit retina. *Albrecht v. Graefes Arch. klin. exp. Ophthalm.* 215(2):71–78
- Beaudoin DL, Manookin MB, Demb JB. 2008. Distinct expressions of contrast gain control in parallel synaptic pathways converging on a retinal ganglion cell. *J. Physiol. (Lond.).* 586(22):5487–5502

This article is protected by copyright. All rights reserved.

- Bloomfield SA, Völgyi B. 2009. The diverse functional roles and regulation of neuronal gap junctions in the retina. *Nat. Rev. Neurosci.* 10(7):495–506
- Brainard DH. 1997. The Psychophysics Toolbox. *Spat Vis.* 10(4):433–36
- Chaffiol A, Ishii M, Cao Y, Mangel SC. 2017. Dopamine Regulation of GABAA Receptors Contributes to Light/Dark Modulation of the ON-Cone Bipolar Cell Receptive Field Surround in the Retina. *Curr. Biol.* 27(17):2600–2609.e4
- Chichilnisky EJ. 2001. A simple white noise analysis of neuronal light responses. *Network.* 12(2):199–213
- Debertin G, Kántor O, Kovács-Öller T, Balogh L, Szabó-Meleg E, et al. 2015. Tyrosine hydroxylase positive perisomatic rings are formed around various amacrine cell types in the mammalian retina. *J. Neurochem.* 134(3):416–28
- Dedek K, Pandarinath C, Alam NM, Wellershaus K, Schubert T, et al. 2008. Ganglion cell adaptability: does the coupling of horizontal cells play a role? *PLoS One.* 3(3):e1714
- Demb JB, Singer JH. 2012. Intrinsic properties and functional circuitry of the All amacrine cell. *Vis Neurosci.* 29(1):51–60
- Dunn FA, Doan T, Sampath AP, Rieke F. 2006. Controlling the gain of rod-mediated signals in the Mammalian retina. *J. Neurosci.* 26(15):3959–70
- Dunn FA, Lankheet MJ, Rieke F. 2007. Light adaptation in cone vision involves switching between receptor and post-receptor sites. *Nature.* 449(7162):603–6
- Enroth-Cugell C, Robson JG. 1966. The contrast sensitivity of retinal ganglion cells of the cat. *Journal of Physiology*
- Farrow K, Teixeira M, Szikra T, Viney TJ, Balint K, et al. 2013. Ambient illumination toggles a neuronal circuit switch in the retina and visual perception at cone threshold. *Neuron.* 78(2):325–38
- Farshi P, Fyk-Kolodziej B, Krolewski DM, Walker PD, Ichinose T. 2016. Dopamine D1 receptor expression is bipolar cell type-specific in the mouse retina. *J. Comp. Neurol.* 524(10):2059–79
- Fein A, Szuts EZ. 1982. *Photoreceptors: Their Role in Vision.* books.google.com
- Flood MD, Eggers ED. 2021. Dopamine D1 and D4 receptors contribute to light adaptation in ON-sustained retinal ganglion cells. *J. Neurophysiol.*
- Flood MD, Moore-Dotson JM, Eggers ED. 2018. Dopamine D1 receptor activation contributes to light-adapted changes in retinal inhibition to rod bipolar cells. *J. Neurophysiol.* 120(2):867–79

- Godley BF, Wurtman RJ. 1988. Release of endogenous dopamine from the superfused rabbit retina in vitro: effect of light stimulation. *Brain Res.* 452(1–2):393–95
- Goel M, Mangel SC. 2021. Dopamine-Mediated Circadian and Light/Dark-Adaptive Modulation of Chemical and Electrical Synapses in the Outer Retina. *Front. Cell Neurosci.* 15:647541
- Goldman ME, Keabian JW. 1984. Aporphine enantiomers. Interactions with D-1 and D-2 dopamine receptors. *Mol. Pharmacol.* 25(1):18–23
- Gong S, Zheng C, Doughty ML, Losos K, Didkovsky N, et al. 2003. A gene expression atlas of the central nervous system based on bacterial artificial chromosomes. *Nature.* 425(6961):917–25
- Grimes WN, Schwartz GW, Rieke F. 2014. The synaptic and circuit mechanisms underlying a change in spatial encoding in the retina. *Neuron.* 82(2):460–73
- Herlinger E, Jameson RF, Linert W. 1995. Spontaneous autoxidation of dopamine. *J. Chem. Soc., Perkin Trans. 2*, p. 259
- Herrmann R, Heflin SJ, Hammond T, Lee B, Wang J, et al. 2011. Rod vision is controlled by dopamine-dependent sensitization of rod bipolar cells by GABA. *Neuron.* 72(1):101–10
- Heukamp AS, Warwick RA, Rivlin-Etzion M. 2020. Topographic variations in retinal encoding of visual space. *Annu. Rev. Vis. Sci.* 6:237–59
- Hoggarth A, McLaughlin AJ, Ronellenfitch K, Trenholm S, Vasandani R, et al. 2015. Specific wiring of distinct amacrine cells in the directionally selective retinal circuit permits independent coding of direction and size. *Neuron.* 86(1):276–91
- Hu EH, Pan F, Völgyi B, Bloomfield SA. 2010. Light increases the gap junctional coupling of retinal ganglion cells. *J. Physiol. (Lond.)*. 588(Pt 21):4145–63
- Huberman AD, Manu M, Koch SM, Susman MW, Lutz AB, et al. 2008. Architecture and activity-mediated refinement of axonal projections from a mosaic of genetically identified retinal ganglion cells. *Neuron.* 59(3):425–38
- Jensen R, Daw N. 1984. Effects of Dopamine Antagonists on Receptive Fields of Brisk Cells and Directionally Selective Cells in the Rabbit Retina. *J. Neurosci.*
- Jensen RJ. 1991. Involvement of glycinergic neurons in the diminished surround activity of ganglion cells in the dark-adapted rabbit retina. *Vis Neurosci.* 6(1):43–53
- Jensen RJ, Daw NW. 1986. Effects of dopamine and its agonists and antagonists on the receptive field properties of ganglion cells in the rabbit retina. *Neuroscience.* 17(3):837–55
- Jouty J, Hilgen G, Sernagor E, Hennig MH. 2018. Non-parametric Physiological Classification of

This article is protected by copyright. All rights reserved.

- Retinal Ganglion Cells in the Mouse Retina. *Front. Cell Neurosci.* 12:481
- Karamanlis D, Gollisch T. 2021. Nonlinear spatial integration underlies the diversity of retinal ganglion cell responses to natural images. *J. Neurosci.* 41(15):3479–98
- Kim T, Shen N, Hsiang JC, Johnson KP, Kerschensteiner D. 2020. Dendritic and parallel processing of visual threats in the retina control defensive responses. *Sci. Adv.* 6(47):
- Kothmann WW, Massey SC, O'Brien J. 2009. Dopamine-stimulated dephosphorylation of connexin 36 mediates All amacrine cell uncoupling. *J. Neurosci.* 29(47):14903–11
- Koulen P. 1999. Postnatal development of dopamine D1 receptor immunoreactivity in the rat retina. *J. Neurosci. Res.* 56(4):397–404
- Kreuz T, Chicharro D, Houghton C, Andrzejak RG, Mormann F. 2013. Monitoring spike train synchrony. *J. Neurophysiol.* 109(5):1457–72
- Kreuz T, Mulansky M, Bozanic N. 2015. SPIKY: a graphical user interface for monitoring spike train synchrony. *J. Neurophysiol.* 113(9):3432–45
- Krieger B, Qiao M, Rousso DL, Sanes JR, Meister M. 2017. Four alpha ganglion cell types in mouse retina: Function, structure, and molecular signatures. *PLoS One.* 12(7):e0180091
- Lee S, Zhang Y, Chen M, Zhou ZJ. 2016. Segregated Glycine-Glutamate Co-transmission from vGluT3 Amacrine Cells to Contrast-Suppressed and Contrast-Enhanced Retinal Circuits. *Neuron.* 90(1):27–34
- Li H, Zhang Z, Blackburn MR, Wang SW, Ribelayga CP, O'Brien J. 2013. Adenosine and dopamine receptors coregulate photoreceptor coupling via gap junction phosphorylation in mouse retina. *J. Neurosci.* 33(7):3135–50
- Maguire G, Werblin F. 1994. Dopamine enhances a glutamate-gated ionic current in OFF bipolar cells of the tiger salamander retina. *J. Neurosci.* 14(10):6094–6101
- Manookin MB, Beaudoin DL, Ernst ZR, Flagel LJ, Demb JB. 2008. Disinhibition combines with excitation to extend the operating range of the OFF visual pathway in daylight. *J. Neurosci.* 28(16):4136–50
- Masland RH. 2012. The neuronal organization of the retina. *Neuron.* 76(2):266–80
- Mazade RE, Eggers ED. 2013. Light adaptation alters the source of inhibition to the mouse retinal OFF pathway. *J. Neurophysiol.* 110(9):2113–28
- Mazade RE, Eggers ED. 2016. Light adaptation alters inner retinal inhibition to shape OFF retinal pathway signaling. *J. Neurophysiol.* 115(6):2761–78

- Mazade RE, Eggers ED. 2020. Inhibitory components of retinal bipolar cell receptive fields are differentially modulated by dopamine D1 receptors. *Vis Neurosci.* 37:E01
- Mazade RE, Flood MD, Eggers ED. 2019. Dopamine D1 receptor activation reduces local inner retinal inhibition to light-adapted levels. *J. Neurophysiol.* 121(4):1232–43
- Münch TA, da Silveira RA, Siegert S, Viney TJ, Awatramani GB, Roska B. 2009. Approach sensitivity in the retina processed by a multifunctional neural circuit. *Nat. Neurosci.* 12(10):1308–16
- Muresan Z, Besharse JC. 1993. D2-like dopamine receptors in amphibian retina: localization with fluorescent ligands. *J. Comp. Neurol.* 331(2):149–60
- Murphy GJ, Rieke F. 2006. Network variability limits stimulus-evoked spike timing precision in retinal ganglion cells. *Neuron.* 52(3):511–24
- Murphy GJ, Rieke F. 2008. Signals and noise in an inhibitory interneuron diverge to control activity in nearby retinal ganglion cells. *Nat. Neurosci.* 11(3):318–26
- Nguyen-Legros J, Simon A, Caillé I, Bloch B. 1997. Immunocytochemical localization of dopamine D1 receptors in the retina of mammals. *Vis Neurosci.* 14(3):545–51
- Nguyen-Legros J, Versaux-Botteri C, Vernier P. 1999. Dopamine receptor localization in the mammalian retina. *Mol. Neurobiol.* 19(3):181–204
- Ogata G, Stradleigh TW, Partida GJ, Ishida AT. 2012. Dopamine and full-field illumination activate D1 and D2-D5-type receptors in adult rat retinal ganglion cells. *J. Comp. Neurol.* 520(17):4032–49
- Pachitariu M, Steinmetz NA, Colonell J. 2018. *Kilosort2*. <https://github.com/MouseLand/>
- Pachitariu M, Steinmetz N, Kadir S, Carandini M, Harris KD. 2016. Kilosort: realtime spike-sorting for extracellular electrophysiology with hundreds of channels. *BioRxiv*
- Pang J-J, Gao F, Wu SM. 2003. Light-evoked excitatory and inhibitory synaptic inputs to ON and OFF alpha ganglion cells in the mouse retina. *J. Neurosci.* 23(14):6063–73
- Pearson JT, Kerschensteiner D. 2015. Ambient illumination switches contrast preference of specific retinal processing streams. *J. Neurophysiol.* 114(1):540–50
- Pelli DG. 1997. The VideoToolbox software for visual psychophysics: transforming numbers into movies. *Spat Vis.* 10(4):437–42
- Pérez-Fernández V, Milosavljevic N, Allen AE, Vessey KA, Jobling AI, et al. 2019. Rod photoreceptor activation alone defines the release of dopamine in the retina. *Curr. Biol.* 29(5):763–774.e5
- Ran Y, Huang Z, Baden T, Schubert T, Baayen H, et al. 2020. Type-specific dendritic integration in

- mouse retinal ganglion cells. *Nat. Commun.* 11(1):2101
- Ribelayga C, Cao Y, Mangel SC. 2008. The circadian clock in the retina controls rod-cone coupling. *Neuron.* 59(5):790–801
- Rivlin-Etzion M, Grimes WN, Rieke F. 2018. Flexible neural hardware supports dynamic computations in retina. *Trends Neurosci.* 41(4):224–37
- Rivlin-Etzion M, Zhou K, Wei W, Elstrott J, Nguyen PL, et al. 2011. Transgenic mice reveal unexpected diversity of on-off direction-selective retinal ganglion cell subtypes and brain structures involved in motion processing. *J. Neurosci.* 31(24):8760–69
- Rossant C, Harris KD. 2013. Hardware-accelerated interactive data visualization for neuroscience in Python. *Front Neuroinformatics.* 7:36
- Rossant C, Kadir SN, Goodman DFM, Schulman J, Hunter MLD, et al. 2016. Spike sorting for large, dense electrode arrays. *Nat. Neurosci.* 19(4):634–41
- Roy S, Field GD. 2019. Dopaminergic modulation of retinal processing from starlight to sunlight. *J Pharmacol Sci.* 140(1):86–93
- Shapley R, Enroth-Cugell C. 1984. Chapter 9 Visual adaptation and retinal gain controls. *Progress in Retinal Research.* 3:263–346
- Strauss S, Korympidou MM, Ran Y, Franke K, Schubert T, et al. 2022. Center-surround interactions underlie bipolar cell motion sensitivity in the mouse retina. *Nat. Commun.* 13(1):5574
- Szikra T, Trenholm S, Drinnenberg A, Jüttner J, Raics Z, et al. 2014. Rods in daylight act as relay cells for cone-driven horizontal cell-mediated surround inhibition. *Nat. Neurosci.* 17(12):1728–35
- Tikidji-Hamburyan A, Reinhard K, Seitter H, Hovhannisyan A, Procyk CA, et al. 2015. Retinal output changes qualitatively with every change in ambient illuminance. *Nat. Neurosci.* 18(1):66–74
- Tikidji-Hamburyan A, Reinhard K, Storchi R, Dietter J, Seitter H, et al. 2017. Rods progressively escape saturation to drive visual responses in daylight conditions. *Nat. Commun.* 8(1):1813
- Tran NM, Shekhar K, Whitney IE, Jacobi A, Benhar I, et al. 2019. Single-Cell Profiles of Retinal Ganglion Cells Differing in Resilience to Injury Reveal Neuroprotective Genes. *Neuron.* 104(6):1039–1055.e12
- van Wyk M, Wässle H, Taylor WR. 2009. Receptive field properties of ON- and OFF-ganglion cells in the mouse retina. *Vis Neurosci.* 26(3):297–308
- Veruki ML. 1997. Dopaminergic neurons in the rat retina express dopamine D2/3 receptors. *Eur J of Neuroscience.* 9(5):1096–1100

- Veruki ML, Wässle H. 1996. Immunohistochemical localization of dopamine D receptors in rat retina. *Eur J of Neuroscience*. 8(11):2286–97
- Vlasits AL, Bos R, Morrie RD, Fortuny C, Flannery JG, et al. 2014. Visual stimulation switches the polarity of excitatory input to starburst amacrine cells. *Neuron*. 83(5):1172–84
- Wang F, Li E, De L, Wu Q, Zhang Y. 2021. OFF-transient alpha RGCs mediate looming triggered innate defensive response. *Curr. Biol*. 31(11):2263–2273.e3
- Warwick RA, Kaushansky N, Sarid N, Golan A, Rivlin-Etzion M. 2018. Inhomogeneous encoding of the visual field in the mouse retina. *Curr. Biol*. 28(5):655–665.e3
- Warwick RA, Riccitelli S, Heukamp AS, Yaakov H, Ankri L, et al. 2022. Top-down modulation of the retinal code via histaminergic neurons of the hypothalamus. *bioRxiv*
- Wei W, Elstrott J, Feller MB. 2010. Two-photon targeted recording of GFP-expressing neurons for light responses and live-cell imaging in the mouse retina. *Nat. Protoc*. 5(7):1347–52
- Witkovsky P. 2004. Dopamine and retinal function. *Doc. Ophthalmol*. 108(1):17–40
- Xin D, Bloomfield SA. 1999. Dark- and light-induced changes in coupling between horizontal cells in mammalian retina. *J. Comp. Neurol*. 405(1):75–87

Additional information

Data availability statement

All relevant data is presented in the figures and the supplementary information. Data are available on request. Please contact the lead author.

The supplementary information can be found on our lab's GitHub repository under the following address: https://github.com/RivlinLab/Dopamine_Retina

This article is protected by copyright. All rights reserved.

Competing interests

The authors declare no competing financial interests.

Author contributions

All authors designed experiments. S.R. performed MEA experiments. A.S.H. analysed MEA experiments. R.A.W. performed patch clamp experiments and analysis. R.A.W, A.S.H. and M.R.-E. wrote the manuscript with input from S.R. All authors edited the manuscript and approved of the final version.

Funding

This project has received funding from the I-CORE (51/11), the Minerva Foundation with funding from the Federal German Ministry for Education and Research, the ISF Foundation (1396/15 and 2449/20), the European Research Council under the European Union's Horizon 2020 research and innovation program (grant agreement no. 757732). We also acknowledge support from the Sagol Weizmann-MIT Bridge Program, Dr. and Mrs. Alan Leshner, the Lubin-Schupf Fund for Women in Science, the Charles and David Wolfson Charitable Trust, Rolf Wiklund and Alice Wiklund Parkinson's disease research fund, Consolidated Anti-Aging Foundation, Dr. Daniel C. Andrae and Ms. Lois Pope. R.A.W. was supported by the Dean of Faculty fellowship and the Koshland Foundation at Weizmann Institute of Science. A.S.H. was supported by the Minerva Fellowship. S.R. was supported by the Dean of Faculty fellowship. M.R.-E. is incumbent of the Sara Lee Schupf Family Chair.

This article is protected by copyright. All rights reserved.